Rhodium(I) and Iridium(I) Complexes of the Conformationally Rigid IBioxMe$_4$ Ligand: Computational and Experimental Studies of Unusually Tilted NHC Coordination Geometries

Jan-Niclas Luy,[a] Simone A. Hauser,[b] Adrian B. Chaplin*,[b] and Ralf Tonner*,[a]

[a] *Fachbereich Chemie, Philipps-Universität Marburg, Hans-Meerwein-Straße 4, D-35032 Marburg, Germany.*

E-mail: Tonner@chemie.uni-marburg.de

[b] *Department of Chemistry, University of Warwick, Gibbet Hill Road, Coventry CV4 7AL, UK.*

Email: a.b.chaplin@warwick.ac.uk

TOC graphic

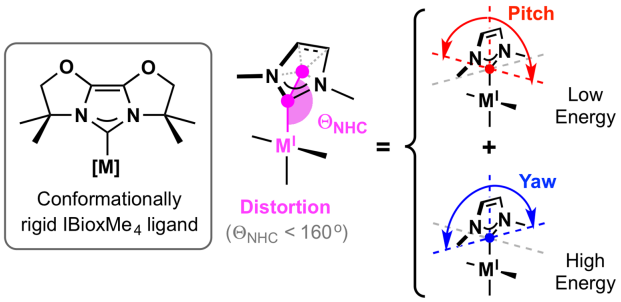

Abstract

Computational methods have been used to analyze distorted coordination geometries in a coherent range of known and new rhodium(I) and iridium(I) complexes containing bioxazoline-based NHC ligands (IBiox). Such distortions are readily placed in context of the literature through measurement of the Cnt(NHC)–C_{NCN}–M angle (Θ_{NHC}; Cnt = ring centroid). On the basis of restricted potential energy calculations using *cis*-[M(IBioxMe$_4$)(CO)$_2$Cl] (**M1**, M = Rh, Ir), in plane (yawing) tilting of the NHC was found to incur significantly steeper energetic penalties than orthogonal out of plane (pitching) movement, which is characterized by noticeably flat potential energy surfaces. Energy Decomposition Analysis (EDA) of the ground state and pitched structures of **M1** indicated only minor differences in bonding characteristics. In contrast, yawing of the NHC ligand is associated with significant increase in Pauli repulsion (i.e. sterics) and reduction in M→NHC π–back donation, but counteracted by supplemental stabilising bonding interactions only possible due to closer proximity of the methyl substituents with the metal and ancillary ligands. Aided by this analysis, comparison to a range of carefully selected model systems and EDA, distorted coordination modes in *trans*-[M(IBioxMe$_4$)$_2$Cl(COE)] (**M2**, M = Rh, Ir) and [M(IBioxMe$_4$)$_3$]$^+$ (**M3**, M = Rh, Ir) have been rationalised. Steric interactions were identified as the major contributing factor and are associated with a high degree of NHC pitching. In the case of **Rh3**, weak agostic interactions also contribute to the distortions, particularly with respect to NHC yawing, and are notable for increasing the bond dissociation energy of the distorted ligands. Supplementing the computational analysis, an analogue of formally 14 VE Rh(I) **Rh3** bearing the cyclohexyl-functionalised IBiox6 ligand ([Rh(IBiox6)$_3$]$^+$, **Rh3-Cy**) was prepared and found to exhibit an exceptionally distorted NHC ligand (Θ_{NHC} = 155.7(2)°) in the solid-state.

Introduction

N-heterocyclic carbenes (NHCs) are widely recognized as a powerful class of ancillary ligand, finding ever-increasing applications in organometallic chemistry and catalysis.[1] In comparison to ubiquitous phosphine ligands, they are characterized by stronger σ-donating properties, orthogonal steric profiles and benefit from numerous, generally straightforward, preparative procedures. The bonding picture for transition metal NHC complexes is well established (Chart 1), consisting primarily of ligand to metal σ-donation and metal to ligand π-back donation.[2,3] These metal-ligand bonding contributions can be quantified using both experimental and computational methods,[4,5] with the determination of Tolman Electronic Parameters and application of Energy Decomposition Analysis (EDA) widely adopted in particular.[6,7]

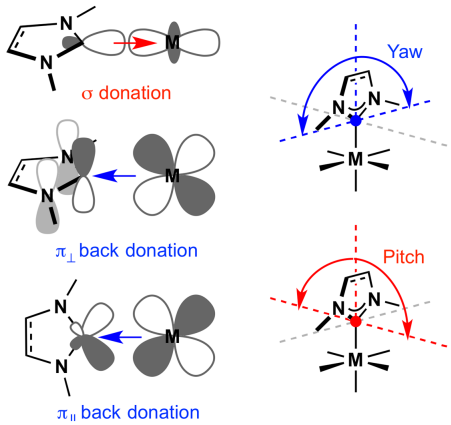

Chart 1. Bonding and tilting in transition metal NHC complexes.

In most previous studies, NHC ligands are generally assumed to bind in a symmetric fashion to the metal center, however in reality, ideal metal-NHC coordination geometries are unusual and instead distortions occur through combinations of in plane (yawing) and out of plane (pitching) tilting (Chart 1). In order to assess the prevalence of such distortions in the solid-state for metal complexes of imidazol-2-ylidene and imidazolin-2-ylidene ligands, we have defined a NHC tilting angle Θ_{NHC} (Cnt(NHC)–C_{NCN}–M; Cnt = ring centroid) to analyze data deposited in the Cambridge Structure Database (CSD, Figure 1). The search revealed that the majority of these commonly employed NHC ligands coordinate within 10° of ideal geometry (all metals, 80.8%; transition metals, 81.9%; platinum group metals, 78.5%), with approximately half within 5° (all metals, 49.1%; transition metals, 50.0%; platinum group metals, 43.5%). The mode was ca. 177°, with a sharp dip in occurrence to higher Θ_{NHC} associated with ideal coordination geometry. Examples of NHC ligands coordinated with $\Theta_{NHC} \leq 160°$ are extremely uncommon (all metals, 1.0%; transition metals, 0.7%; platinum group metals, 0.6%). In the case of metal systems with $\Theta_{NHC} \leq 170°$, most are characterized by a high degree of yawing (72.9% with $|\angle_{MCN} - \angle_{MCN'}| > 15°$); by inspection, examples showing such pronounced yawing involve chelating NHC ligands (e.g. **A**, Figure 1).[8] Notable examples of extremely distorted, but non-chelated, NHC ligands include main group complexes reported by Jones and Krossing (e.g. **B**) and alkaline metal complexes prepared by Schumann (e.g. **C**).[9] Of the platinum group

metals, the most distorted (non-chelated) examples to our knowledge have been identified in a rhodium complex bearing the 7,9-bis(2,6-diisopropylphenyl)-6b,9a-dihydroacenaphtha[1,2-d]imidazolin-2-ylidene ligand (**D**, Θ_{NHC} = 153.3(3)° / 155.2(3)° [Z' = 2], Figure 1): excluding those discussed herein, all others are characterized by Θ_{NHC} > 158°.[10,11]

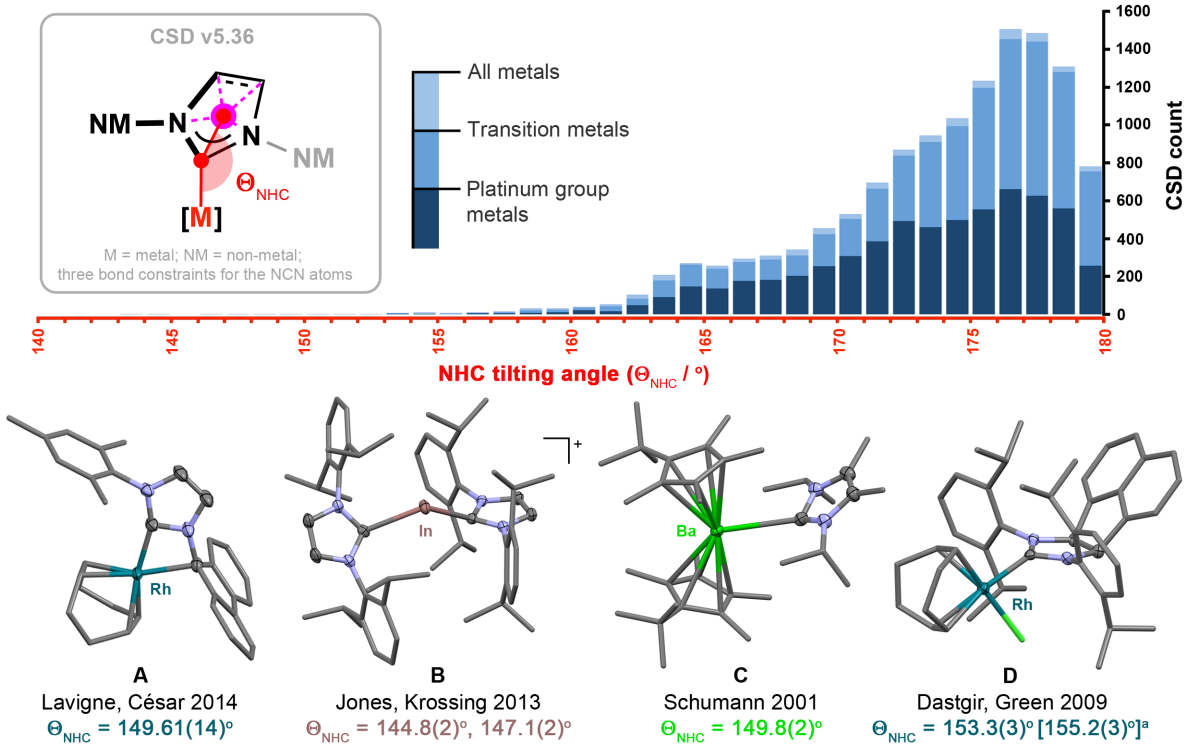

Figure 1. Structural data for NHC complexes deposited in the CSD.

With a view of exploring the organometallic chemistry of low-coordinate NHC complexes of rhodium and iridium, some of us have recently begun to expand the coordination chemistry of Glorius' bioxazoline-based variants (IBiox),[12] seeking to exploit the conformationally rigid nature of these ligands to avoid intramolecular cyclometalation reactions that can occur via C–H bond activation of the downward pointing alkyl and aryl NHC appendages.[13] In particular, we have focused our initial efforts on studying the coordination chemistry of IBioxMe$_4$, which shares many structural similarities with the commonly employed I^{t}Bu ligand; a NHC that has been shown to undergo cyclometalation reactions when partnered with reactive late transition metal fragments (Scheme 1).[14] Through this approach we have been successful in isolating low-coordinate, formally 14 VE rhodium(I) complexes and generating highly reactive Ir(I) analogues in solution that undergo facile, selective and reversible intermolecular C–H bond activation of fluoroarenes rather than cyclometalation of the IBioxMe$_4$ ligand.[15,16] Interestingly, during the course of our investigations it was also observed that the IBioxMe$_4$ ligand can adopt highly distorted NHC coordination geometries, characterized by values of Θ_{NHC} down to 156.5(2)°.[15]

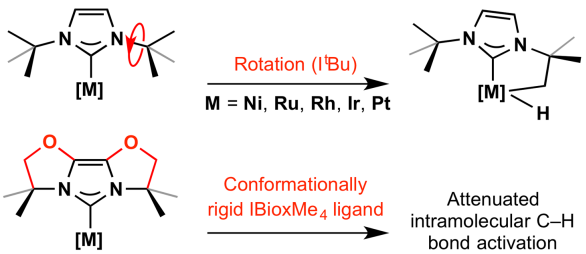

Scheme 1. Hypothesized reactivity modulation using IBiox ligands.

Seeking to fully understand the tilted geometries possible with the IBioxMe$_4$ ligand, in this report we describe our attempts to quantify and delineate the underlying steric and electronic effects. After discussing the two conformations observed for the free NHC ligand, the known mono-ligated IBioxMe$_4$ complexes *cis*-[M(IBioxMe$_4$)(CO)$_2$Cl] (**M1**, M = Rh, Ir) are analysed. The energetics associated with both yawing and pitching of the NHC ligand in these relatively simple systems is probed and the EDA method used to assess how the metal-ligand bonding is affected by such distortions. Using the resulting metrics, and comparisons to carefully selected structural analogues, the tilted geometries observed experimentally in the solid-state structures of *trans*-[M(IBioxMe$_4$)$_2$(COE)Cl] (**M2**, M = Rh, Ir; COE = cyclooctene) and then [Rh(IBioxMe$_4$)$_3$]$^+$ (**Rh3**) are analysed in turn. The findings not only provide valuable insights into the coordination chemistry of IBioxMe$_4$, but can be generalized to other NHC ligands. The preparation and structural characterization of an analogue of **Rh3**, containing instead a bulkier cyclohexyl IBiox ligand [Rh(IBiox6)$_3$]$^+$ (**Rh3-Cy**), is additionally reported and helps substantiate trends elucidated from the previously reported IBioxMe$_4$ systems.

Results

Conformations of IBioxMe$_4$

Puckering of the 5-membered oxazoline rings leads to two different conformational isomers of the IBioxMe$_4$ ligand, which feature either staggered or eclipsed arrangements of the downward pointing methyl groups (Figure 2). The optimized geometries of both isomers have very similar structural parameters, and although the C_2 symmetrical staggered isomer is found to be more stable, the calculated energy difference is less than 1 kJ mol^{-1} using both density functional theory (BP86/TZ2P) and wave function based (MP2/TZVPP) approaches (Figure 2b). In both isomers, the C–C bond lengths of the methyl groups orientated perpendicular to the imidazolylidene rings are elongated by ca. 0.01 Å, as a consequence of interactions with electron density on the NCN moiety (negative hyperconjugation) stemming from the HOMO (Figure 2c). The staggered conformation and effects of negative hyperconjugation are observed experimentally in the solid-state structure of the pro-ligand (IBioxMe$_4$·HOTf), however, consistent with the very small energy difference calculated, eclipsed and disordered mixtures of staggered/eclipsed conformers are observed in the solid-state structures of other substituted IBiox pro-ligands.[12c]

The electronic similarity of the two IBioxMe$_4$ isomers is further underlined by inspection of the frontier orbitals relevant to coordination (Figure 2c): the HOMO-1 (sp^2-type nonbonding electron pair at carbene-C)

and LUMO (p-type orbital at carbene-C) exhibit energy differences of less than 0.05 eV in the respective isomers. The σ-donor and π-acceptor character of the two conformations should therefore be very similar. It is interesting to note that the HOMO is not the σ-donor orbital, but an orbital representing mainly the donation of electron density from the nonbonding electron pairs of the nitrogen atoms into the formally empty p-orbital at carbon. This is a reverse orbital ordering compared to the parent NHC (imidazol-2-ylidene).[7b] The large coefficient at the carbene-C in the LUMO points toward a good π-acceptor ability of the ligand.

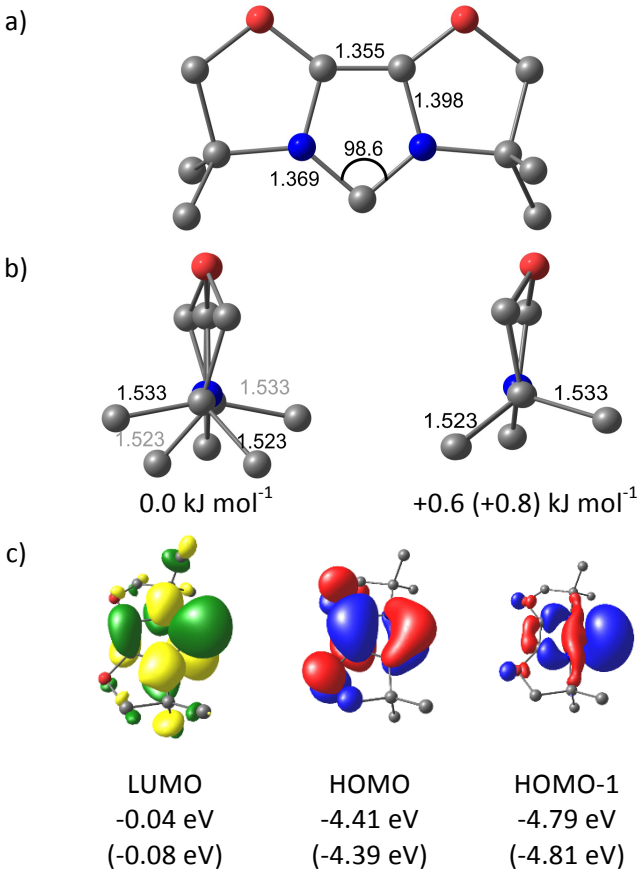

Figure 2. a) Front (staggered only) and b) side views of staggered (left) and eclipsed (right) conformations of the $IBioxMe_4$ ligand (bond lengths in Å, angles in °). Energy differences are derived from BP86/TZ2P and MP2/TZVPP//BP86/TZ2P (in brackets). c) Frontier orbitals and energies (BP86/TZ2P) for staggered conformer; equivalent values for the eclipsed conformer in brackets.

Mono-ligated complexes: *cis*-[M(IBioxMe$_4$)(CO)$_2$Cl]

The mono-ligated IBioxMe$_4$ complexes *cis*-[M(IBioxMe$_4$)(CO)$_2$Cl] (**M1**, M = Rh, Ir) were chosen to help evaluate the energetics associated with both yawing and pitching of the NHC ligand as they are relatively simple systems with non-bulky co-ligands. The solid-state structure of **Rh1** has previously been reported and shows no significant tilting of the IBioxMe$_4$ ligand (Θ_{NHC} = 179.0(2)°).[15b] As the IBioxMe$_4$ ligand adopts an eclipsed geometry experimentally in **Rh1** we have focused only on computational models of **M1'** with this conformation for simplicity (Figure 3).[17] Although the iridium system has been prepared, it is yet to be structurally characterized in the solid-state.[12c] Instead, the closely related IBiox derivate carrying cyclohexyl groups [Ir(IBiox6)(CO)$_2$Cl] (**Ir1-Cy** – staggered, Θ_{NHC} = 179.5(4)°) was used to authenticate the geometry of the computed structure of **Ir1'**.[12c]

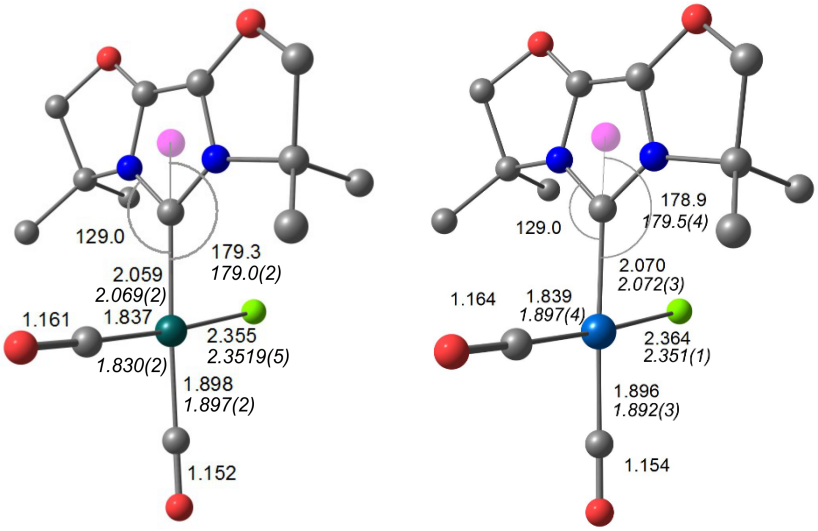

Rh1' **Ir1'**

Figure 3. Optimized structures of **Rh1'** and **Ir1'** (BP86/TZ2P). Distances in Å, angles in °. Selected experimental data from Refs. 15b (**Rh1**) and 12c (**Ir1-Cy**) given in italics.

As validation of the model chemistry employed throughout our studies, the computed structural metrics show good agreement with the aforementioned experimental precedents (Figure 3). Moreover, the absolute computed stretching frequencies for **Rh1'** (2048.5, 1975.5 cm^{-1}) and **Ir1'** (2043.4, 1970.1 cm^{-1}) are in qualitative agreement with experimental data recorded in CH_2Cl_2 solution (**Rh1**, 2081, 2000 cm^{-1}; **Ir1**, 2066, 1982 cm^{-1}), with relative trends preserved. To give an estimate of the error, the theoretically derived value of ν(CO) for free carbon monoxide is 2122 cm^{-1} (cf. 2143 cm^{-1}) at this computational level.

Since reorientation of the NHC's substituents by simple (low-energy) rotation about the N–C bond is not possible in IBiox ligands, unfavourable steric interactions can only be relieved through tilting of the entire ligand. The energetic consequences for such distortions were investigated by computing restricted potential energy surfaces (rPESs) for yawing and pitching tilting of the IBioxMe$_4$ ligand in **M1'**, by a rigid

scan of the respective reaction coordinate (Figure 4). Yawing notably leads to a significantly steeper rPES compared to pitching.[18] For instance, at a pitching angle of 30° the energetic penalty is less than 50 kJ mol^{-1}, while a yawing angle of 30° leads to calculated increases in energy of over 200 kJ mol^{-1}. NHC yawing angles more commonly associated with experimental data (around 10°) lead to increases in energy of less than 20 kJ mol^{-1}. Combined, these data indicate that rather large pitching and moderate yawing movements are energetically accessible for the IBioxMe$_4$ ligand.

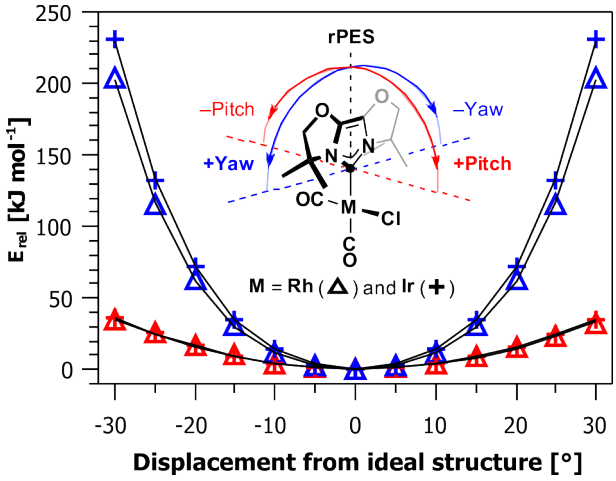

Figure 4. Restricted potential energy (rPES) curves for pitching (red) and yawing (blue) of IBioxMe$_4$ in **M1'**. Solid lines represent polynomial fits.[18]

The yawing rPES for **Ir1'** is steeper compared to **Rh1'**, although the effect is small. These and other differences can be understood by EDA of the metal-ligand interactions using the optimized structures **Rh1'** and **Ir1'** (Table 1) together with the Natural Orbitals for Chemical Valence (NOCV) extension of the method. The dissociation energies ($D_e = -\Delta E_{bond}$) for the IBioxMe$_4$ ligand are 297.1 kJ mol^{-1} (**Rh1'**) and 315.3 kJ mol^{-1} (**Ir1'**), indicating stronger bonding of the NHC with iridium as expected based on the enhanced bonding characteristics of third vs. second row transition metals (*vide infra*). These metrics are much more reliable than absolute bond lengths in evaluating bond strength: the calculated M–NHC bond distance is actually shorter for rhodium (2.057 vs. 2.070 Å). In both cases the attractive terms making up the intrinsic energy of the metal-ligand interaction (ΔE_{int}) after preparation of the fragments (ΔE_{prep}) consist of 70% electrostatic (ΔE_{elstat}) and 30% orbital (ΔE_{orb}) energies. The iridium complex shows larger values for both attractive energy terms and is therefore stronger bonded than the rhodium complex, although Pauli repulsion is also higher in **Ir1'**. Important deformation densities for **Rh1'** in the ground state are shown in Figure 5 (similar are observed for **Ir1'**). The first deformation density represents σ-donation ($\Delta\rho_1$), while π-back donation consists of three components: $\Delta\rho_2$ and $\Delta\rho_3$ show the π–back donation perpendicular to the NHC plane ($\pi_\perp$ component in Chart 1), while $\Delta\rho_4$ highlights π–back donation into the in-plane acceptor orbitals of the NHC ($\pi_\parallel$ component in Chart 1). Together these results help quantify the established view that the metal-ligand interaction is dominated by σ-donation (around 2/3) in **M1'**, with minor but important π-back donation (around 1/3) contributions (only the total π–back donation ΔE_π is listed in Table 1). Associated with the

calculated dissociation energies (ΔE_{bond}), the absolute values of the σ and π components are larger for **Ir1'** compared to **Rh1'**.

In addition to the ground state structure of **Rh1'**, an EDA of selected structures from the rPES of the rhodium complex was also carried out to gain insight into the changes in bonding induced on pitching and yawing of the $IBioxMe_4$ ligand (at 20°, Table 1, Figure 5). For the pitched structures, the changes are all very minor in agreement with the shallow nature of the rPES associated with this movement. Pitching toward the CO ligand is only marginally less favourable (ca. 3 kJ mol^{-1} at 20° from ΔE_{int}). The yawed structures show a reduction of the metal-ligand interaction by ca. 60 kJ mol^{-1}. Interestingly, this is not due to reduced total orbital or electrostatic interactions as the values for these contributions increase by ca. 37 and 27 kJ mol^{-1}, respectively. These enhancements can be explained by inspection of the deformation densities for the yawed structure (Figure 5), which show the formation of C-H···Rh ($\Delta\rho_3$, $\Delta E_{\rho 3}$ = -31.6 kJ mol^{-1}; $\Delta\rho_5$, $\Delta E_{\rho 5}$ = -11.4 kJ mol^{-1} (not shown)) and C-H···Cl interactions ($\Delta\rho_4$, $\Delta E_{\rho 4}$ = -17.7 kJ mol^{-1}) due to close proximity of the methyl groups with the metal centre. The absolute value of the σ-donation contribution decreases marginally on yawing, but the major change is found for the π–back donation, which decreases by 22 kJ mol^{-1}. Nevertheless, this is overcompensated by the C-H···Rh and C-H···Cl interactions of the methyl groups. The main reason for the weakening of the metal-NHC bond (and the steep rPES) on yawing is a large (21%) increase in the Pauli repulsion (i.e. sterics).

Rh1' (opt)

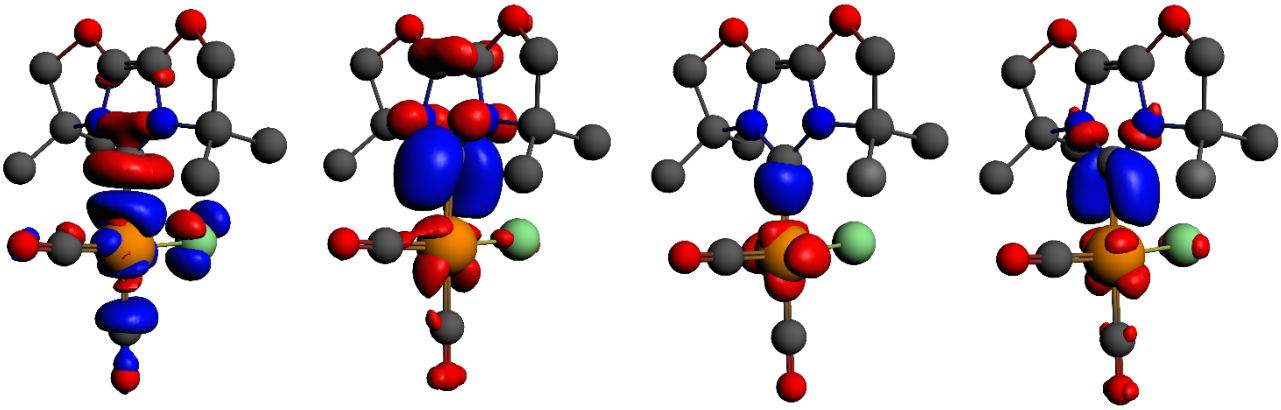

$\Delta\rho_1$
$\Delta E_{\rho 1}$ = -207.5 kJ mol^{-1}
ν_1 = 0.730
σ-donation

$\Delta\rho_2$
$\Delta E_{\rho 2}$ = -28.1 kJ mol^{-1}
ν_2 = 0.262
$\pi_\perp$ back donation

$\Delta\rho_3$
$\Delta E_{\rho 3}$ = -21.5 kJ mol^{-1}
ν_3 = 0.187
$\pi_\perp$ back donation

$\Delta\rho_4$
$\Delta E_{\rho 4}$ = -14.9 kJ mol^{-1}
ν_4 = 0.150
$\pi_\parallel$ back donation

Rh1' (20° yaw).

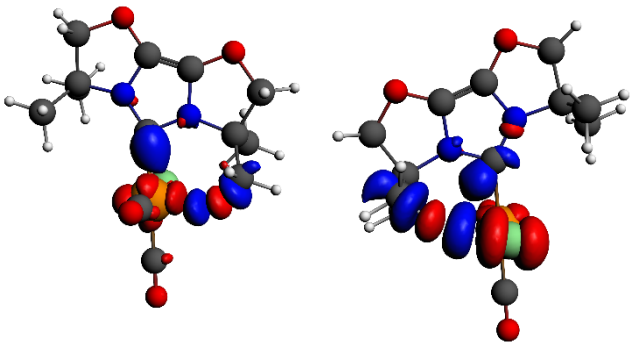

$\Delta\rho_3$
$\Delta E_{\rho 3}$ = -31.6 kJ mol^{-1}
ν_3 = 0.233
C-H···Rh interaction

$\Delta\rho_4$
$\Delta E_{\rho 4}$ = -17.7 kJ mol^{-1}
ν_1 = 0.160
C-H···Cl interaction

Figure 5. Selected deformation densities $\Delta\rho$ for **Rh1'** in optimized (top) and 20° yawed (bottom) structures from EDA-NOCV analysis together with eigenvalues ν for NOCV orbitals, corresponding energy values ΔE_ρ and interpretation of the $\Delta\rho$-character. The yawed structure is shown in different perspectives to highlight the important interactions. Charge flow from red to blue.

Table 1. EDA results for **M1'** – fragmentation **M1'** → IBioxMe$_4$ + M(CO)$_2$Cl (M = Rh, Ir). All values in units of kJ mol^{-1}.

	Rh1'								**Ir1'**	
	opt		pitch (Cl)[a]		pitch (CO)[a]		yaw[a]		opt	
ΔE_{int}	-326.4		-312.2		-309.4		-265.2		-370.2	
ΔE_{disp}	-62.8		-66.5		-62.2		-66.8		-66.1	
ΔE_{Pauli}	745.0		748.5		723.1		874.1		900.4	
ΔE_{elstat} [b]	-705.9	(70%)	-687.6	(69%)	-668.3	(69%)	-732.7	(68%)	-845.7	(70%)
ΔE_{orb} [b]	-302.7	(30%)	-306.6	(31%)	-301.9	(31%)	-339.9	(32%)	-358.7	(30%)
ΔE_{σ} [c]	-207.5	(68%)	-207.7	(67%)	-211.2	(69%)	-203.0	(59%)	-251.1	(70%)
	0.730		0.732		0.752		0.729		0.711	
ΔE_{π} [c]	-64.4	(21%)	-64.5	(21%)	-61.7	(20%)	-42.4	(12%)	-77.8	(22%)
	0.600		0.599		0.579		0.399		0.722	
$\Delta E_{CH\cdots X}$ [c]							-60.7	(18%)		
							0.514			
$\Delta E_{resid.}$ [c]	-34.5	(11%)	-38.0	(12%)	-32.1	(11%)	-37.7	(11%)	-32.3	(9%)
ΔE_{prep}	29.4		29.5		29.5		29.4		54.8	
ΔE_{prep} (L)	5.6		5.7		5.6		5.6		5.7	
ΔE_{prep} (M)	23.8		23.9		23.9		23.8		49.1	
ΔE_{bond} (=-D_e)	-297.1		-282.7		-279.9		-235.8		-315.3	

[a] The EDA was carried out for selected points on the rPES for **Rh1'**: pitch (Cl) is the structure with a pitching angle of +20° (toward Cl), pitch (CO) is the structure with a pitching angle of -20° (toward CO), yaw is a structure with a yawing angle of 20° (both directions give equivalent results).

[b] The percentage values give the contribution to the total attractive interactions $\Delta E_{elstat} + \Delta E_{orb}$.

[c] The percentage values give the contribution to the total orbital interaction ΔE_{orb}. The character of the interaction is deduced from visual inspection of the NOCV orbitals; eigenvalues (ν) are given below the energy values. $\Delta E_{CH\cdots X}$ consists of CH···X interactions with X = Cl, Rh as shown in Figure 5.

Increased steric pressure: *trans*-[M(IBioxMe$_4$)$_2$Cl(alkene)]

In the preceding experimental work with IBioxMe$_4$, the most distorted NHC coordination geometries observed were noted in the bis-NHC complex *trans*-[Rh(IBioxMe$_4$)$_2$Cl(COE)] **Rh2**.[15b] The solid-state structure contained two independent molecules (i.e. *Z'* = 2), one with both NHC ligands staggered (Θ_{NHC} = 170.1(3), 164.7(3)°) and the other both eclipsed (Θ_{NHC} = 173.0(2), 156.5(2)°). Because of the symmetry of the co-ligands, this distortion is almost pure pitching in both cases ($|\angle_{MCN} - \angle_{MCN'}| < 3°$). The iridium analogue **Ir2** has also recently been described,[16] and we now report its solid-state structure (Figure 6). In this case only the all-staggered isomer is observed and in line with the steeper rPESs associated with **Ir1'** in comparison to **Rh1'**, reduced NHC tilting is observed (Θ_{NHC} = 176.8(3), 167.0(2)°). Related iridium systems [Ir(NHC)$_2$Cl(COE)] (5 examples) have been reported by Nolan and co-workers and are characterized by $\Theta_{NHC} \geq 170°$.[19] Interestingly, a pronounced twisting of the coordinated COE ligand is found in the solid-state structure of **Ir2** (staggered) (|C26-Ir1-Cnt(C3,C4)-C4| = 76.88(17)°). A similar twist, but of reduced magnitude, is seen in **Rh2** (staggered) (82.70(18)°), but is absent from **Rh2** (eclipsed), which instead shows essentially ideal perpendicular coordination of the COE ligand (89.70(17)°).[20] In all examples the most distorted IBioxMe$_4$ ligands are those interacting most strongly with the coordinated COE ligand (i.e the lower ligands, orientated as shown in Figure 6) and they show elongated M–C_{NCN} bond lengths in comparison to the other NHC ligand ($\Delta_{M\text{-}NCN}$: **Rh2** (eclipsed), 0.074(4) Å; **Rh2** (staggered), 0.017(4) Å; **Ir2** (staggered), 0.026(4) Å).

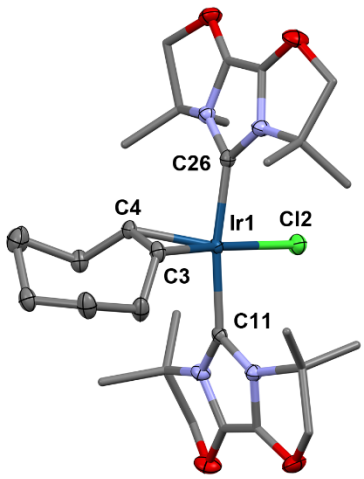

Figure 6. Solid-state structure of **Ir2** (staggered). Thermal ellipsoids for selected atoms are drawn at the 50% probability level; minor disordered component and solvent molecule omitted for clarity. Selected bond lengths (Å) and angles(°) (computed values at BP86/TZ2P given in italics): Ir1-Cl2, 2.3858(5) *(2.396)*; Ir1-C3, 2.147(2) *(2.157)*; Ir1-C4, 2.107(2) *(2.118)*; Ir1-C11, 2.067(2) *(2.030)*; Ir1-C26, 2.041(2) *(2.050)*; C3-C4, 1.423(3) *(1.432)*; Cl2-Ir1-Cnt(C3,C4), 172.78(6) *(173.73)*; C11-Ir1-C26, 170.17(8) *(170.53)*; Θ_{NHC}(@C11), 167.0(2) *(169.1)*; Θ_{NHC}(@C26), 176.8(3) *(177.8)*.

In order to computationally probe the effect of steric pressure on the NHC tilting in these bis-NHC systems we have optimized the structures of the all-staggered and all-eclipsed isomers of **M2'** and two model systems where the coordinated COE ligand is replaced with ethylene, i.e. [M(IBioxMe$_4$)$_2$Cl(C_2H_4)] (all-eclipsed; M = Rh, Ir; **M4'**). The structural parameters are given in Figure 7 and the caption of Figure 6. The

agreement is generally very good, especially with respect to tilting (e.g. Θ_{NHC} for the most titled NHC in **Rh2'** (eclipsed) = 159.0 vs. 156.5(2)°). This is quite remarkable due to the flat PES for the pitching and underlines the validity of the computational approach even for these sensitive bond parameters.

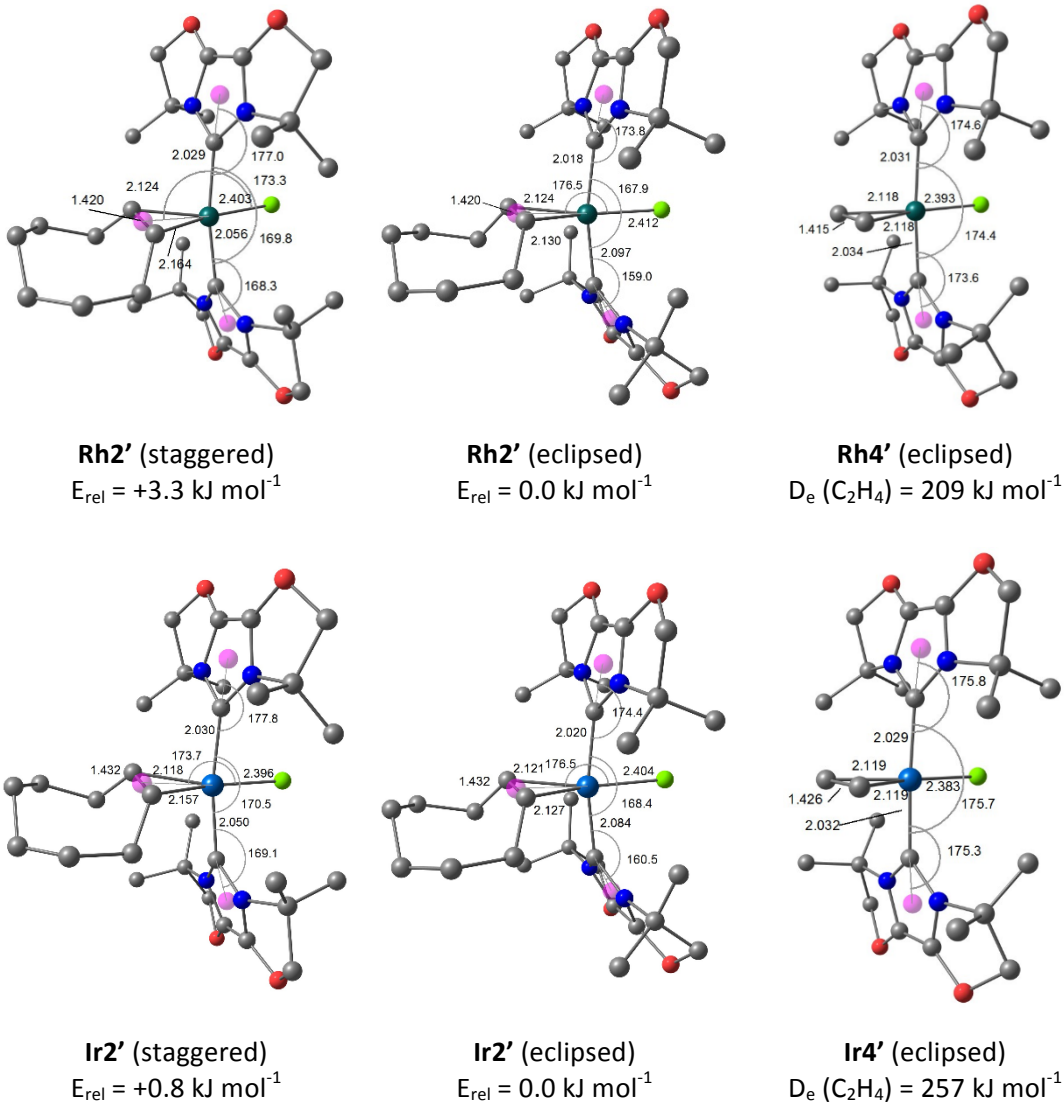

Rh2' (staggered)
E_{rel} = +3.3 kJ mol^{-1}

Rh2' (eclipsed)
E_{rel} = 0.0 kJ mol^{-1}

Rh4' (eclipsed)
D_e (C_2H_4) = 209 kJ mol^{-1}

Ir2' (staggered)
E_{rel} = +0.8 kJ mol^{-1}

Ir2' (eclipsed)
E_{rel} = 0.0 kJ mol^{-1}

Ir4' (eclipsed)
D_e (C_2H_4) = 257 kJ mol^{-1}

Figure 7. Optimized structures of isomers of **M2'** and **M4'** (BP86/TZ2P). Distances in Å, angles in °.

For both central metals, the all-eclipsed conformation of **M2'** is the most stable, but the energy differences are very small (**Rh2'** 3.3 kJ mol^{-1}; **Ir2'** 0.8 kJ mol^{-1}). This result is at first a little surprising, given the eclipsed geometry of the free ligand is (albeit marginally) higher energy and these conformations are associated with the most pronounced distortion of the IBioxMe$_4$ ligands (i.e. Θ_{NHC} = 159.0° (**Rh2'**), 160.5° (**Ir1'**) for the lower ligands as orientated in Figure 7). The large pitching of the lower IBioxMe$_4$ ligands in these systems is clearly in direct response to steric pressure imposed by the coordinated COE ligand (i.e. clashes with the CH=CHC<u>H$_2$</u> methylene groups) and readily evidenced by the distinctly different Θ_{NHC} values for the two *trans*-disposed NHC ligands. In the all-staggered isomers of **M2**, the orientation of the methyl groups of IBioxMe$_4$ results in an asymmetric steric profile for the coordinated COE ligand and necessitates an

energetically unfavourable twisting of the alkene ligand out of the plane; features which are well reproduced in the optimized structures **M2'** (twist angle as defined above: 77.0° (**Rh2'**) and 77.5° (**Ir2'**)). There is still a degree of NHC tilting present in the staggered isomers, but it is considerably less than the eclipsed analogues (ca. 10° less, equivalent to ca. 4.6 kJ mol^{-1} as determined from the polynomial fit to rPES in Fig. 4).[18] Ultimately, based on the relative energies of the isomers, the pitching appears to be the most energetically accessible means for minimising the steric clashes between the COE and NHC ligands. However, it is worth re-emphasising the differences in energy are very small for both rhodium and iridium. Indeed, given the magnitude of the energy differences calculated here, the observation of either conformational isomer in the solid-state is most likely dictated by subtle crystal packing effects rather than any fundamental difference in electronic structure.

To further reinforce the aforementioned observations, the less sterically congested model complexes **M4'** (eclipsed) are useful comparisons. The replacement of the COE ligand with ethylene leads to essentially undistorted coordination of the NHC ligands (i.e. Θ_{NHC} = 173.6, 174.6 (**Rh4'**); 175.3, 175.8 (**Ir4'**)). Using **M4'** as a reference point, the COE ligand not only leads to distortion of the NHC, but to compression of the C_{NCN}-M-C_{NCN} angle by ca. 7°. Associated with the tilting of NHC ligands in **M2'** (eclipsed), the M–C_{NCN} bonds for the lower $IBioxMe_4$ ligands are lengthened considerably compared to **M4'** (ca 0.06 Å), a change which is compensated by a shorting of the *trans*-M–C_{NCN} bonds (ca. 0.01 Å). Similar, but less pronounced effects are seen in **M2'** (staggered) – in line with the less distorted NHC geometries observed.

As a side note, the ethylene ligand is found to bind more strongly to iridium (D_e = 257 kJ mol^{-1}) compared to rhodium (D_e = 209 kJ mol^{-1}). This is in line with the experimental finding that the reaction of **Rh2** with excess $IBioxMe_4$ results in formation of $[Rh(IBioxMe_4)_3Cl]$ via a dissociative mechanism.[15b] In contrast, no reaction is observed between **Ir2** and excess $IBioxMe_4$, even on prolonged heating at elevated temperature.[16]

Distortions in $[M(IBiox)_3]^+$

In the previously reported formally 14 VE, T-shaped complex $[Rh(IBioxMe_4)_3]^+$ **Rh3**, strong distortions of the mutually *trans*-$IBioxMe_4$ ligands were observed and characterized by values of Θ_{NHC} as low as 160.0(3)°.[15] Such distortions are absent in related coordinatively saturated analogues $[Rh(IBioxMe_4)_3(L)]^+$ (L = CO, **Rh5**; Cl^-, **Rh6**). To investigate the relative role of steric and electronic effects on the twisting of the $IBioxMe_4$ ligand further we have used these compounds as another coherent experimental data set (Chart 2).[21] The iridium analogues are also of interest, however, the high reactivity of **Ir3** proved to be prohibitive during previous attempts in its isolation.[16] We now report the preparation of the carbonyl complex $[Ir(IBioxMe_4)_3(CO)][BAr^F_4]$ **Ir5** (Ar^F = 3,5-$C_6H_3(CF_3)_2$) which is readily prepared by placing $[Ir(IBioxMe_4)_3(NCCH_3)][BAr^F_4]$ under an atmosphere of CO and was isolated in 95% yield. The structure of the new complex was fully verified spectroscopically in solution and in the solid-state by X-ray diffraction –

as for **Rh5** no significant NHC tilting is found (all Θ_{NHC} > 175; Figure 8). Despite our continued efforts we have, however, been unable to prepare **Ir6** (e.g. no reaction is observed between **Ir2** and $IBioxMe_4$).[16] In addition to computational models centred on experimental precedents (Figure 9), **Rh3-H1'**, **Rh3-H2'** and **Rh3-H3'** (Figure 10) were also included to probe steric, agostic and electronic effects *in silico*. In all cases, only all-staggered isomers were targeted based on the X-ray data for **M5** and **Rh6**. The solid-state structure of **Rh3** contains primarily staggered $IBioxMe_4$ ligands also, however, each independent cation features one staggered/eclipsed disordered $IBioxMe_4$ ligand (Z' = 2).[15]

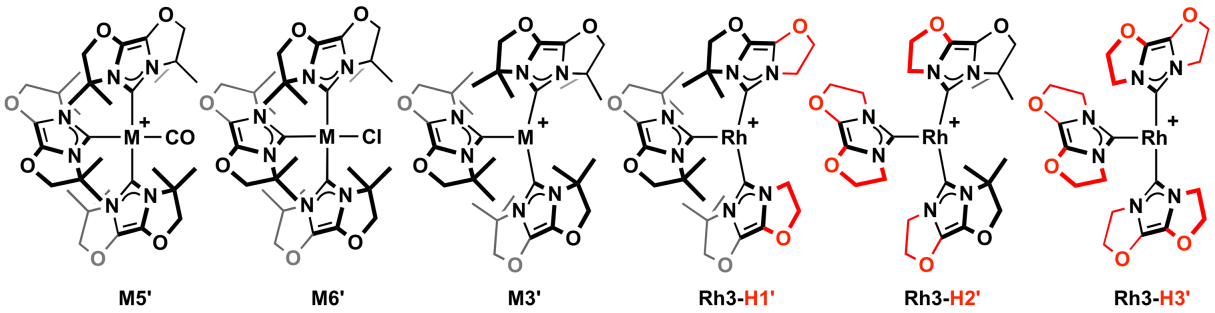

Chart 2. $[M(IBiox)_3]^+$ complexes investigated (M = Rh, Ir).

Again, the agreement between the computed structures and the respective experimental data is very good (Figure 8). The vibrational mode of the carbonyl ligand in **Ir5** is significantly lower than in **Rh5** (1958 vs. 1968 cm^{-1}), as expected based on the enhanced back bonding characteristics of third row transition metals, and this feature is well reproduced computationally (**Ir5'**: 1958.7 cm^{-1}, **Rh5'**: 1961.4 cm^{-1}).

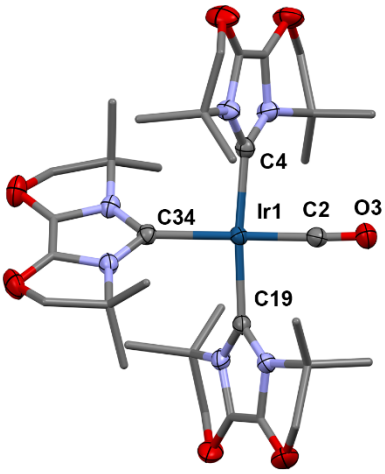

Figure 8. Solid-state structure of **Ir5**. Thermal ellipsoids for selected atoms are drawn at the 50% probability level; minor disordered components, solvent and anion omitted for clarity. Selected bond lengths (Å) and angles(°) (computed values at BP86/TZ2P given in italics): Ir1-C2, 1.836(5) *(1.860)*; Ir1-C4, 2.062(3) *(2.053)*; Ir1-C19, 2.072(3) *(2.056)*; Ir1-C34, 2.156(3) *(2.083)*; C2-Ir1-C34, 177.1(3) *(175.92)*; C4-Ir1-C19, 173.64(13) *(176.26)*; all Θ_{NHC} > 175 (*>178*).

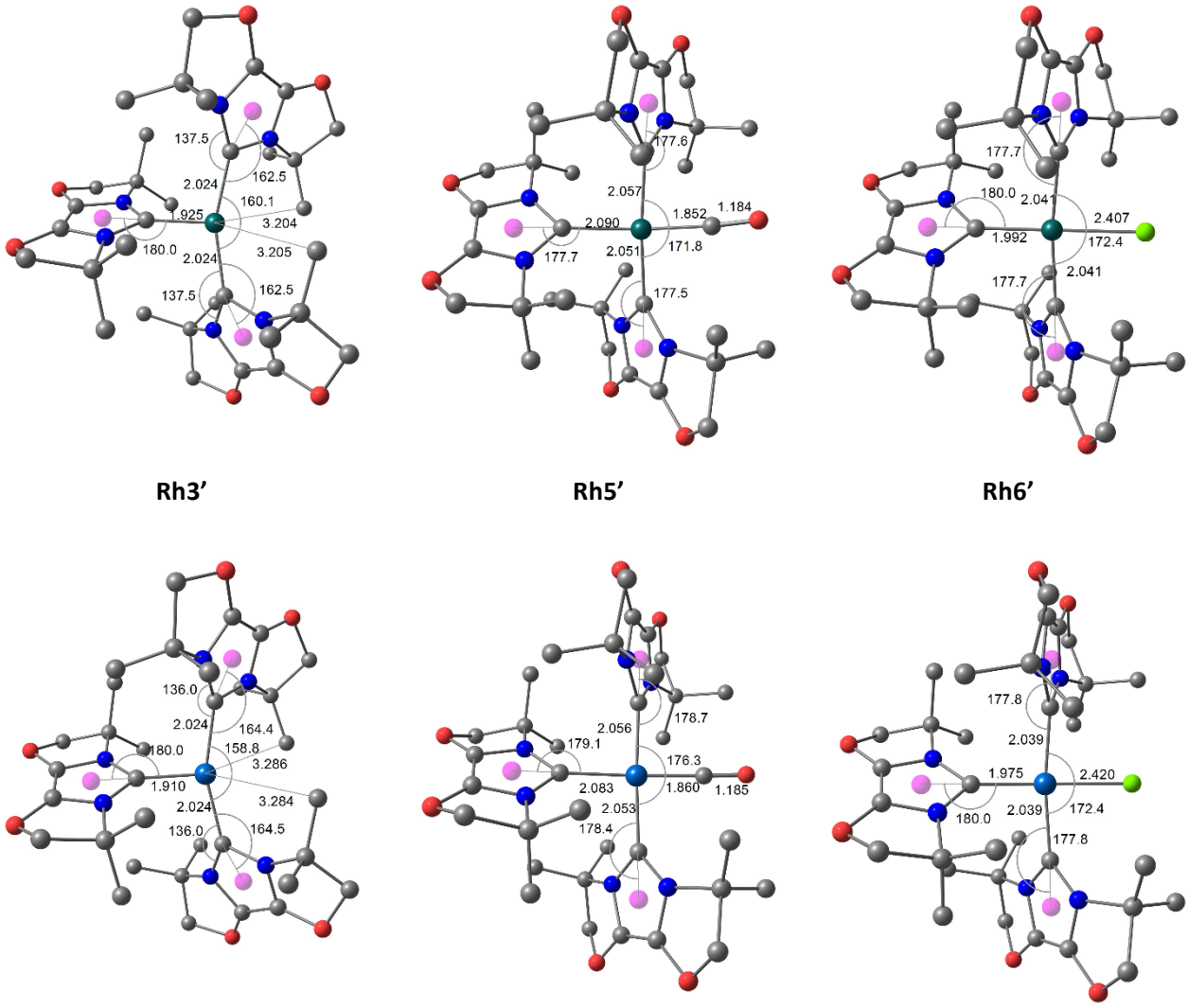

Figure 9. Optimized structures of **M3'**, **M5'** and **M6'** (BP86/TZ2P). Distances in Å, angles in °.

The interaction between the most-tilted carbene ligand and the metal fragment in each of **M3'**, **M5'** and **M6'** was investigated using the EDA method. The results are summarized in Table 2 and selected deformation densities for **Rh3'** are shown in Figure 11 (and are representative for the orbital interaction components in the series). The results indicate that the strongest of the respective metal-carbene bonds are in the low-coordinate complexes, with the bond dissociation energies decreasing in the order **M3'** > **M5**' > **M6'**. This trend is accounted for by the high preparation energy terms for the metal fragments containing CO and Cl^- co-ligands despite, for example, the intrinsic bond–energy being greater for **M5'** compared to **M3'**. As for **M1'**, these results further highlight the metal-ligand bond lengths are not reliable indicators of bond dissociation energy (nor intrinsic interaction energy).

The EDA features are comparable to model complexes **M1'**. As shown above, pitching does not lead to major changes in the bonding pattern; the model complexes can thus be compared even though exhibiting different degrees of pitching. The attractive contributions to the interaction energy (ΔE_{int}) show a similar ratio of electrostatic (approx. 70%) to orbital terms (approx. 30%) in the model complexes similar to

optimized **M1'** and pitched **Rh1'**. The interaction with two IBioxMe$_4$ ligands in **M3'** leads to higher dispersion energy contribution in comparison to the interaction with CO and Cl ligands in **M1'** ($\Delta\Delta E_{disp}$(**M1'**–**M3'**) = 44.0 kJ mol^{-1} (M = Rh), 44.3 kJ mol^{-1} (M = Ir)). This leads to similar interaction energies in **M3'** and **M1'**, although **M3'** exhibits higher Pauli repulsion due to the proximity of the three IBioxMe$_4$ ligands. The dispersion contributions in **M5'** and **M6'** are even slightly higher since less pitching in these complexes leads to an even closer proximity of the three IBioxMe$_4$ ligands. The iridium complexes exhibit stronger metal-ligand bonds in all cases as has been found for **M1'**. This can be understood when analysing the major contributions to the orbital interaction term as shown by the deformation densities from NOCV analysis (Figure 11). The major orbital interactions are comparable to **M1'**: σ-donation ($\Delta\rho_1$) making up approx. 50% of the orbital interaction and π-donation ($\Delta\rho_2$, $\Delta\rho_3$, $\Delta\rho_6$) contributing 25-28%. With the latter again being composed of in-plane and out-of-plane components. As for **M1'**, the absolute σ and π contributions are also considerably stronger for Ir than for Rh, although the ratios remain similar. The σ-type interaction is comparable in **M3'** and **M6'**, while showing higher absolute and relative contributions in **M5'** even though the metal-ligand bond is longer by ca. 0.02-0.03 Å. Along the series the π-interaction is strongest in the low-coordinate complexes **M3'** and weakest in **M5'**, presumably because the CO ligand is competing for the d-orbitals on the metal centre.

Table 2. EDA results for **M3', M5'** and **M6'** (M = Rh, Ir) – fragmentation of the most tilted IBioxMe$_4$ ligand. Energies in kJ mol^{-1} and distances in Å.

	Rh3'		**Rh5'**		**Rh6'**		**Ir3'**		**Ir5'**		**Ir6'**	
ΔE_{int}	-318.6		-332.7		-288.0		-363.8		-379.3		-324.6	
ΔE_{disp}	-106.8		-125.8		-130.0		-110.4		-130.6		-133.4	
ΔE_{Pauli}	863.1		828.7		889.1		1106.3		1030.0		1096.5	
ΔE_{elstat} [a]	-740.3	(69%)	-709.3	(68%)	-731.9	(70%)	-937.7	(69%)	-880.5	(69%)	-907	(70%)
ΔE_{orb} [a]	-334.5	(31%)	-326.3	(32%)	-315.3	(30%)	-422	(31%)	-398.4	(31%)	-380.7	(30%)
ΔE_{σ} [b]	-160.7	(48%)	-183.9	(56%)	-162.0	(51%)	-217.1	(51%)	-236.8	(59%)	-212.5	(56%)
	0.688		0.682		0.636		0.714		0.691		0.661	
ΔE_{π} [b]	-95.6	(29%)	-77.7	(24%)	-83.7	(27%)	-118.1	(28%)	-100.0	(25%)	-106.7	(28%)
	0.703		0.660		0.760		0.766		0.827		0.957	
$\Delta E_{CH\cdots X}$ [b,c]	-31.1	(9%)			-13.1	(4%)	-36.0	(9%)			-8.6	(2%)
	0.338				0.137		0.395				0.116	
$\Delta E_{resid.}$ [b]	-47.2	(14%)	-64.7	(20%)	-56.3	(18%)	-50.8	(12%)	-61.6	(15%)	-52.8	(14%)
ΔE_{prep}	8.4		89.9		86.6		38.2		93.2		111.0	
ΔE_{bond} (=-D_e)	-310.2		-242.8		-201.4		-325.6		-286.1		-213.6	
d(M-L)	2.024		2.057		2.044		2.024		2.056		2.039	

[a] The percentage values give the contribution to the total attractive interactions $\Delta E_{elstat} + \Delta E_{orb}$.
[b] The percentage values give the contribution to the total orbital interaction ΔE_{orb}. The character of the interaction is deduced from visual inspection of the NOCV orbitals; eigenvalues (ν) are given below the energy values.
[c] Agostic interaction for **M3'** (X = Rh, Ir), C–H···Cl interaction for **M6'** (i.e. X = Cl).

Additional orbital contributions are found in **M3'** and **M6'**. In the low coordinate complexes, a weak agostic interaction between the methyl groups of the IBioxMe$_4$ ligand and the metal centre contributes 9% to the total orbital interaction ($\Delta\rho_4$, $\Delta\rho_5$ in Figure 11). The calculated M···HC distances are 3.204/3.205 Å (**Rh3'**); 3.284/3.286 Å (**Ir3'**) and the corresponding C–H bonds are elongated by ca. 0.017 Å. The absolute values suggest a slightly stronger agostic interaction in the Ir system (E_{orb}: -31.1 vs. -36.0 kJ mol^{-1}). In **M6'** the Cl ligand can engage in a C–H···Cl interaction comparable to the one noted in **M1'** delivering a small stabilising contribution (ca. 3%) to the orbital interaction term.

To further understand the energetic relevance of the agostic interactions in the ligand distortions observed experimentally in **Rh3**, the optimized structures of **Rh3-H1'**, **Rh3-H2'** and **Rh3-H3'** are useful *in silico* constructs (Figure 10, Figure 11, Table 3). Complex **Rh3-H1'** maintains the steric pressure of the parent complex, but selective removal of methyl groups from the mutually *trans* IBiox ligand precludes the formation of any agostic interactions. This perturbation leads to a small change in the total NHC distortion observed in the mutually *trans* NHC ligands Θ_{NHC} = 169.1° (cf. 162.5°) and the associated C_{NCN}–Rh–C_{NCN} angle (**Rh3-H1'**, 163.9°; **Rh3'**, 160.1°). There is, however, a notable reduction in the extent of yawing in the mutually *trans* IBioxMe$_4$ ligands in **Rh3-H1'** (i.e. $|\angle_{MCN} - \angle_{MCN'}|$: **Rh3-H1'**, 11.2° vs. **Rh3'**, 18.0°). This change reflects that the ca. 32 kJ mol^{-1} (based on **M1'**, Figure 4, derived from polynomial fit)[18] penalty

associated with yawing can no longer be balanced by formation of agostic interaction ($E_{agostic}$ ca. 31 kJ mol^{-1} in **Rh3'**, Table 2). The absence of the agostic interaction contributes noticeably to the decrease in the bond dissociation energy compared to the parent complex (D_e = 279.8 vs. 310.2 kJ mol^{-1}, Table 3).

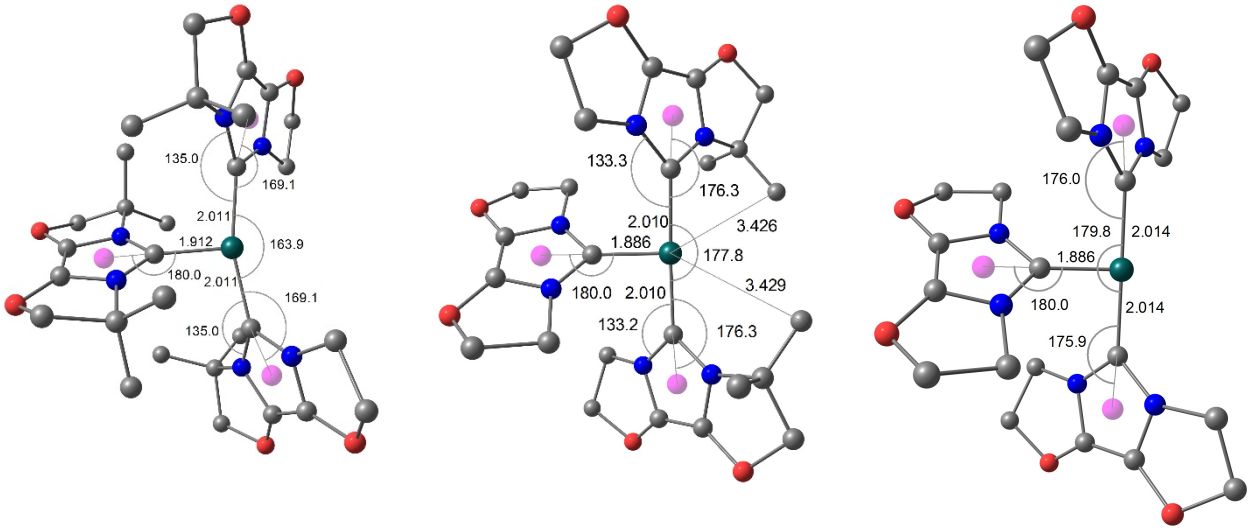

Rh3-H1' **Rh3-H2'** **Rh3-H3'**

Figure 10. Models derived from **Rh3'** strategically substituting methyl groups by hydrogen. Distances in Å, angles in °.

In the model complex **Rh3-H2'** all but the methyl groups in close proximity to the metal centre have been removed from the IBioxMe$_4$ ligands, reducing the steric pressure but leaving the possibility for agostic interactions. The optimized structure of **Rh3-H2'** is however notable for reduced Rh···HC contacts (**Rh3-H2'**, 3.426/3.429 vs. 3.204/3.205 Å) and elongation of the respective C-H bonds of 0.009 Å (cf. 0.017 Å), compared to **Rh3'**. Both metrics indicate even weaker agostic interactions are adopted and supported by EDA ($E_{agostic}$, -17.6 vs. -31.1 kJ mol^{-1}; and D_e, 298.6 vs. 310.2 kJ mol^{-1}; Table 3). Correspondingly, there is little yawing of the mutually *trans* IBioxMe$_4$ ligands in **Rh3-H2'** (i.e. $|\angle_{MCN} - \angle_{MCN'}|$: **Rh3-H2'**, 7.0°; **Rh3'**, 18.0°). Moreover, in comparison to **Rh3'** the mutually *trans* NHC ligands in **Rh3-H2'** exhibit little total distortion (Θ_{NHC} = 176.3° vs. 162.5°) and a more linear C_{NCN}–Rh–C_{NCN} angle is adopted (177.8° vs. 160.1°). A second slightly higher energy isomer of **Rh3-H2'** (+1.7 kJ mol^{-1}) with a different relative orientation of the IBioxMe$_2$H$_2$ ligands was also optimized containing one strong agostic interaction (Figure S1, Table S1; $E_{agostic}$ = -55.5 kJmol^{-1}, D_e = 296.9 kJmol^{-1}). This interaction is characterized by a short Rh···HC contact of 2.753 Å and significant C-H bond elongation (0.035 Å) more typical of agostic interactions.[22] The associated NHC is significantly distorted (Θ_{NHC} = 162.0°) with a high degree of yawing (i.e. $|\angle_{MCN} - \angle_{MCN'}|$ = 22.8°).

Table 3. EDA results for **Rh3-Hx'** (x = 0, 1, 2, 3) – fragmentation of the most-tilted IBioxMe$_4$ ligand. Energies in kJ mol^{-1} and distances in Å.

	Rh3'	**Rh3-H1'**	**Rh3-H2'**	**Rh3-H3'**
ΔE_{int}	-318.6	-303.8	-310.9	-298.9
ΔE_{disp}	-106.8	-79.0	-65.5	-50.7
ΔE_{Pauli}	863.1	804.5	759.3	721.9
ΔE_{elstat} [a]	-740.3 (69%)	-731.1 (71%)	-715.9 (71%)	-698.1 (72%)
ΔE_{orb} [a]	-334.5 (31%)	-298.2 (29%)	-288.8 (29%)	-272.0 (28%)
ΔE_{σ} [b]	-160.7 (48%)	-170.6 (57%)	-154.7 (53%)	-151.8 (56%)
	0.688	0.876	0.622	0.616
ΔE_{π} [b]	-95.6 (29%)	-93.6 (31%)	-82.2 (28%)	-97.1 (36%)
	0.703	0.705	0.715	0.567
$\Delta E_{agostic}$ [b]	-31.1 (9%)		-17.6 (6%)	
	0.338		0.167	
$\Delta E_{resid.}$ [b]	-47.2 (14%)	-35.7 (12%)	-34.9 (12%)	-23.0 (8%)
ΔE_{prep}	8.4	24.0	12.2	15.6
ΔE_{bond} (=-D_e)	-310.2	-279.8	-298.6	-283.3
d(M-L)	2.024	2.011	2.010	2.014

[a] The percentage values give the contribution to the total attractive interactions $\Delta E_{elstat} + \Delta E_{orb}$.
[b] The percentage values give the contribution to the total orbital interaction ΔE_{orb}. The character of the interaction is deduced from visual inspection of the NOCV orbitals; eigenvalues (ν) are given below the energy values.

For reference, removal of all the methyl groups leads to essentially an ideal non-distorted geometry for **Rh3-H3'** (i.e. Θ_{NHC} > 175° and C_{NCN}–M–C_{NCN} = 179.8°). Combined, these results highlight that distortion from ideal NHC coordination geometry observed experimentally in **Rh3** is the consequence of steric clashes between the mutually *cis*-IBioxMe$_4$ ligands; weak agostic interactions result in only a small perturbation to the geometry. A suggestion quantified through EDA, with Pauli repulsion terms decreasing with successive removal of methyl substituents (Table 3) and reinforced by the trend in optimized M-C_{NCN} bond lengths of the IBiox ligand *trans* to the free coordination site: **Rh3'** (1.925 Å) > **Rh3-H1'** (1.912 Å) > **Rh3-H2'** = **Rh3-H3'** (1.886 Å). The range of NHC geometries found in **Rh3-Hx'** (x = 0, 1, 2, 3) lead to differences in the orbital interaction terms. The σ-donation is the leading term in all cases and larger for **Rh3-H1'** compared to **Rh3'**. The π-back donation is similar throughout and only drops for **Rh3-H2'** slightly. The structures with even weak agostic interactions are, however, ultimately associated with greater dissociation energies (D_e): **Rh3'** (310.2 kJ mol^{-1}) > **Rh3-H2'** (298.6 kJ mol^{-1}) > **Rh3-H3'** (283.3 kJ mol^{-1}) ≈ **Rh3-H1'** (279.8 kJ mol^{-1}). Dispersion stabilization (ΔE_{disp}) is a major contribution to the higher stability for **Rh3'**, which also exhibits a smaller preparation energy (ΔE_{prep}). Notably, bond lengths show a different trend (**Rh3'** > **Rh3-H3'** > **Rh3-H1'** ≈ **Rh3-H2'**) and are again not reliable indicators for the bond strength.

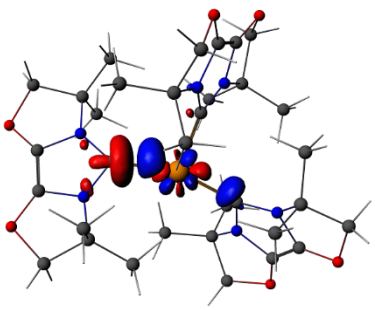

$\Delta\rho_1$
$\Delta E_{\rho 1}$ = -160.7 kJ mol^{-1}
ν_1 = 0.688
σ-donation

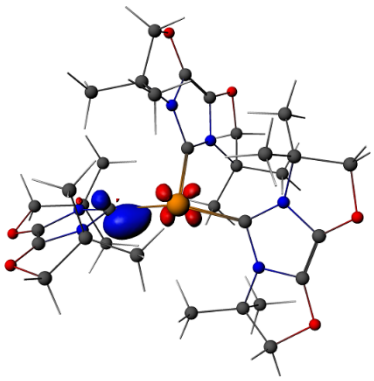

$\Delta\rho_2$
$\Delta E_{\rho 2}$ = -58.1 kJ mol^{-1}
ν_2 = 0.397
$\pi_{\perp}$ back donation

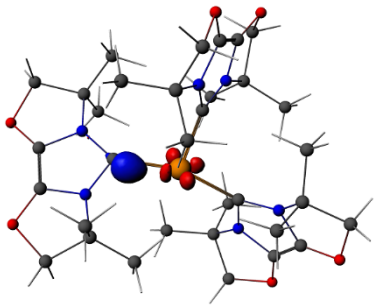

$\Delta\rho_3$
$\Delta E_{\rho 3}$ = -29.1 kJ mol^{-1}
ν_3 = 0.205
$\pi_{\parallel}$ back donation

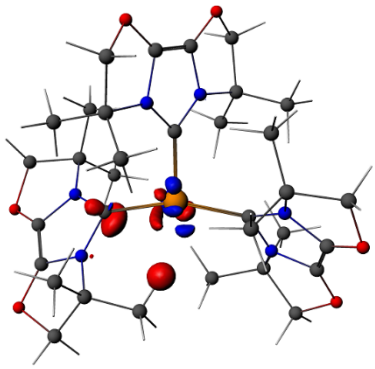

$\Delta\rho_4$
$\Delta E_{\rho 4}$ = -14.4 kJ mol^{-1}
ν_4 = 0.179
weak agostic

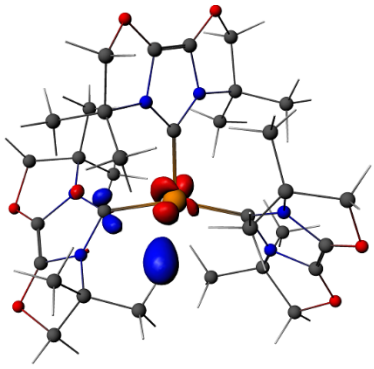

$\Delta\rho_5$
$\Delta E_{\rho 5}$ = -16.7 kJ mol^{-1}
ν_5 = 0.159
weak agostic

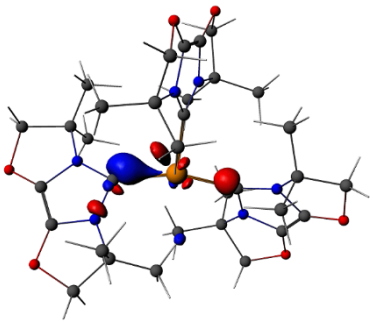

$\Delta\rho_6$
$\Delta E_{\rho 6}$ = -8.4 kJ mol^{-1}
ν_6 = 0.101
$\pi_{\parallel}$ back donation

Figure 11. Deformation densities $\Delta\rho$ for **Rh3'** from EDA-NOCV analysis together with eigenvalues ν for NOCV orbitals, corresponding energy values ΔE_ρ and interpretation of the $\Delta\rho$-character. Charge flow is from red to blue.

Synthesis and isolation of [Rh(IBiox6)$_3$][BAr$^F{}_4$] (Rh3-Cy)

With the body of computational evidence supporting facile and sterically induced tilting of the IBioxMe$_4$ ligand in rhodium and iridium complexes, we decided to experimentally test these assertions through preparation of a more sterically congested analogue of **Rh3**, bearing instead the cyclohexyl-functionalised IBiox ligand IBiox6 (Chart 3), to induce more pronounced ligand distortions. The required free carbene ligand was readily formed by reaction of the imidazolium pro-ligand IBiox6·HOTf, synthesised in four steps as previously described by Glorius and co-workers,[12b,c] with the strong hindered base K[N(SiMe$_3$)$_2$] in THF. In this manner, IBiox6 was isolated in 84% yield, following removal of volatiles in vacuo and extraction with benzene, and stored under argon in a glove box. Satisfactory microanalyses were obtained and the free carbene was fully characterized in C_6D_6 solution by NMR spectroscopy. C_{2v} symmetry is observed in solution at room temperature with the carbene resonance at 191.1 ppm, consistent with IBioxMe$_4$ and other ligands.[15,23] Following a directly analogous procedure to that for **Rh3**, involving reaction of [Rh(COE)$_2$Cl]$_2$ with IBiox6 in 1,2-$C_6H_4F_2$ using Na[BAr$^F{}_4$] as a halide abstractor, led to the isolation of **Rh3-Cy** in 69% yield. In common with **Rh3**, the new homoleptic complex is stable on extended standing in either CD_2Cl_2 or 1,2-$C_6H_4F_2$ (48 hours at 293 K) and exhibits time-averaged D_3 symmetry in solution (500 MHz, 298 K). The solid-state structure of **Rh3-Cy** bears close resemblance to **Rh3**, with a pseudo T-shaped geometry (Figure 12). The closest Rh1···HC distance of 3.182(4) Å (calc. 3.150 Å) suggests the presence of no significant/weak agostic interactions; the corresponding C–H bond is elongated by ca. 0.02 Å in the calculated structure, although the close proximity of the C–H bond to the rhodium is an inevitable consequence of the sterically crowded nature of the complex. In comparison to **Rh3**, gratifyingly, the mutually *trans* NHC ligands show a significantly greater degree of tilting (Θ_{NHC} = 155.7(2), 160.4(2)° cf. 163.9(3), 173.1(3) / 160.0(3), 166.5(3)° [Z' = 2]) in line with the hypothesis. The distortions are closely reproduced in the optimized structure (BP86/TZVPP). To our knowledge, only **D** (Θ_{NHC} = 153.3(3)° / 155.2(3)° [Z' = 2]) shows more distorted NHC coordination geometries in platinum group complexes.

Chart 3. IBiox6 ligand.

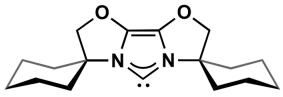

IBiox6
(84% isolated yield)

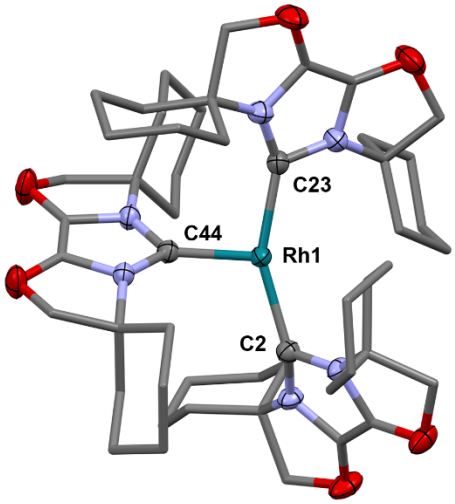

Figure 12. Solid-state structure of **Rh3-Cy**. Thermal ellipsoids for selected atoms are drawn at the 50% probability level; anion omitted for clarity. Selected bond lengths (Å) and angles(°) (computed values at BP86/TZVPP given in italics): Rh1-C2, 2.060(3) (*2.016*); Rh1-C23, 2.008(3) (*2.015*); Rh1-C44, 1.942(3) (*1.921*); closest Rh1···HC(IBiox6), 3.182(4) (*3.150*); C2-Rh1-C23, 153.24(13) (*152.2*); Θ_{NHC}(@C2), 155.7(2) (*154.2*); Θ_{NHC}(@C23), 160.4(2) (*154.1*); Θ_{NHC}(@C44), 173.5(2) (*179.9*).

Summary and Outlook

Seeking to fully understand the capacity of bioxazoline-based NHC ligands (IBiox) to adopt distorted, non-ideal coordination geometries in late transition metal complexes, computational methods have been used to quantify and delineate the underlying steric and electronic effects in a coherent range of known and new mono-, bis-, and tris-ligated rhodium(I) and iridium(I) systems. Since reorientation of the NHC's substituents by rotation about the N–C bond is not possible in these fused ring ligands; unfavourable steric interactions can only be relieved through combinations of in plane (yawing) and out of plane (pitching) tilting of the entire NHC ligand that we have quantified through measurement of the Cnt(NHC)–C_{NCN}–M angle (Θ_{NHC}). Using *cis*-[M(IBioxMe$_4$)(CO)$_2$Cl] (**M1**, M = Rh, Ir), significantly large pitching (ca. 20°), but only moderate yawing movements (ca. 10°) were found to be energetically accessible for the IBioxMe$_4$ ligand (20 kJ mol^{-1} penalty). Energy Decomposition Analysis (EDA) of the ground state and pitched structures of **M1** indicated only minor differences in the bonding characteristics. In contrast, yawing of the NHC ligand is associated with significant increase in Pauli repulsion (i.e. sterics) and reduction in M→NHC π–back donation, but counteracted by supplemental stabilising bonding interactions only possible due to closer proximity of the methyl substituents with the metal and ancillary ligands. Aided by this analysis, the range of distorted IBioxMe$_4$ geometries observed experimentally in *trans*-[M(IBioxMe$_4$)$_2$Cl(COE)] (**M2**, M = Rh, Ir; Θ_{NHC} = 156.5(2) – 176.8(3)°) are attributed to subtle conformational differences of the oxazoline rings and the ability to minimise steric repulsions between the coordinated COE ligand and methyl substituents of the IBioxMe$_4$ ligand through NHC pitching. In contrast the optimized geometries of *trans*-[M(IBioxMe$_4$)$_2$Cl(C$_2$H$_4$)] (**M4'**, M = Rh, Ir) show almost symmetrical metal-NHC geometries. In the more sterically congested and low-coordinate [M(IBioxMe$_4$)$_3$]$^+$ (**M3**, M = Rh, Ir) complexes, ligand distortions

were rationalised through comparison and EDA of coordinatively saturated adducts $[M(IBioxMe_4)_3(L)]^+$ (M = Rh, Ir; L = CO, **M5**; Cl^-, **M6**) and, in the case of rhodium, hypothetical systems involving strategic removal of methyl substituents from the NHC ligands (**Rh3-Hx'**; x = 1, 2, 3). Focusing in particular on the previously isolated and characterized **Rh3**, steric interactions were identified as the major contributing factor to the distortions found for the mutually *trans*-$IBioxMe_4$ ligands. Weak agostic interactions also contribute to the distortions, particularly with respect to NHC yawing, and are notable for increasing the bond dissociation energy of the distorted ligands. On the basis of the computational analysis of **M1** – **M6**, an analogue of formally 14 VE Rh(I) **Rh3**, bearing the cyclohexyl-functionalised IBiox ligand ($[M(IBiox6)_3]^+$, **Rh3-Cy**) was prepared and found to exhibit an exceptionally distorted NHC ligand (Θ_{NHC} = 155.7(2)°).

Together, these results showcase the capacity of NHCs generally to adopt non-ideal coordination geometries and highlight design principles that may enable the reactivity of NHC complexes to be tuned through for instance, chelating architectures or conformationally rigid NHC appendages.

Experimental

Synthetic details

All manipulations were performed under an atmosphere of argon using Schlenk and glove box techniques. Glassware was oven dried at 130°C overnight and flamed under vacuum prior to use. Anhydrous CH_2Cl_2, C_6H_6, heptane, THF and acetonitrile (<0.005 % H_2O) were purchased from ACROS or Aldrich and freeze-pump-thaw degassed three times before being placed under argon. CD_2Cl_2 was dried over CaH_2 and vacuum distilled. $[Rh(COE)_2Cl]_2$,[24] $[Ir(IBioxMe_4)_2(COE)Cl]$,[16] $[Ir(IBioxMe_4)_3(NCCH_3)][BAr^F_4]$,[16] IBiox6·OTf[12c] and $Na[BAr^F_4]$[25] were prepared as previously described. NMR spectra were recorded on Bruker DPX-400 and AVIIIHD-500 spectrometers at 298 K. ^1H NMR spectra recorded in 1,2-$C_6H_4F_2$ were referenced using the highest intensity peak of the highest frequency fluoroarene multiplet (δ 6.87). Chemical shirts are quoted in ppm and coupling constants in Hz. Microanalyses were performed by Stephan Boyer at London Metropolitan University.

$[Ir(IBioxMe_4)_2(COE)Cl]$ (Ir2)

Single crystals suitable for X-ray diffraction were obtained from slow diffusion of heptane into a solution of **Ir2** in C_6H_6 at room temperature.

$[Ir(IBioxMe_4)_3(CO)][BAr^F_4]$ (Ir5)

A solution of $[Ir(IBioxMe_4)_3(NCCH_3)][BAr^F_4]$ (0.016 g, 0.009 mmol) in acetonitrile (1 mL) was placed under CO (1 atm). After 2 hours at room temperature, the volatiles were removed under vacuum. The resulting solid was recrystallised from CH_2Cl_2 – heptane (10 mL) to afford the crystalline product upon diffusion. Yield = 0.015 g (95%, yellow crystals).

^{1}H NMR (CD_2Cl_2, 400 MHz): δ 7.70 – 7.74 (m, 8H, Ar^F), 7.56 (br, 4H, Ar^F), 4.49 (d, $^2J_{HH}$ = 8, 2H, OCH_2), 4.48 (d, $^2J_{HH}$ = 8, 2H, OCH_2), 4.43 (d, $^2J_{HH}$ = 8, 2H, OCH_2), 4.42 (d, $^2J_{HH}$ = 8, 2H, OCH_2), 4.39 (d, $^2J_{HH}$ = 8, 2H, OCH_2), 4.25 (d, $^2J_{HH}$ = 8.4, 2H, OCH_2), 2.13 (s, 6H, CH_3), 2.05 (s, 6H, CH_3), 1.98 (s, 6H, CH_3), 1.63 (s, 6H, CH_3), 0.93 (s, 6H, CH_3), 0.83 (s, 6H, CH_3). **^{13}C{^{1}H} NMR** (CD_2Cl_2, 101 MHz): δ 183.4 (s, CO), 162.3 (q, $^1J_{BC}$ = 50, Ar^F), 157.0 (s, NCN), 148.5 (s, 2×NCN), 135.4 (s, Ar^F), 129.4 (qq, $^2J_{FC}$ = 32, $^3J_{BC}$ = 3, Ar^F), 127.6 (s, $\underline{C}OCH_2$), 127.4 (s, $\underline{C}OCH_2$), 126.8 (s, $\underline{C}OCH_2$), 125.2 (q, $^1J_{FC}$ = 272, Ar^F), 118.0 (sept, $^3J_{FC}$ = 4, Ar^F), 89.5 (s, OCH_2), 88.8 (s, OCH_2), 87.6 (s, OCH_2), 67.2 (s, $\underline{C}(CH_3)_2$), 64.9 (s, $\underline{C}(CH_3)_2$), 62.4 (s, $\underline{C}(CH_3)_2$), 27.1 (s, CH_3), 26.7 (s, 2×CH_3), 25.4 (s, CH_3), 24.5 (s, CH_3), 21.9 (s, CH_3). **Anal.** Calcd for $C_{66}H_{60}BF_{24}IrN_6O_7$ (1708.23 gmol^{-1}): C, 46.41; H, 3.54; N, 4.92. Found: C, 46.51; H, 3.48; N, 5.04. **IR** (CH_2Cl_2, cm^{-1}): ν(CO) 1958.

IBiox6

To a mixture of IBiox6·HOTf (2.68 g, 6.1 mmol) and K[N($SiMe_3$)$_2$] (1.28 g, 6.4 mmol) was added ice cold THF (30 mL) and the resulting suspension stirred at room temperature for 60 minutes. The volatiles were thoroughly removed in vacuo (> 2 hour at < 1 × 10^{-2} mbar). The residue was extracted with benzene (30 mL) and the product obtained following removal of the solvent from the combined fractions. Yield = 1.48 g (84%, off-white powder).

^{1}H NMR (C_6D_6, 500 MHz): δ 4.11 (s, 4H, OCH_2), 2.05 – 2.14 (m, 4H, Cy), 1.88 (br, 4H, Cy), 1.52 – 1.61 (m, 4H, Cy), 1.15 – 1.26 (m, 4H, Cy), 0.89 – 1.00 (m, 4H, Cy). **^{13}C{^{1}H} NMR** (C_6D_6, 126 MHz): δ 191.1 (s, NCN), 123.6 (s, $\underline{C}OCH_2$), 85.8 (s, OCH_2), 61.2 (s, $COCH_2\underline{C}$), 36.3 (Cy), 25.4 (Cy), 23.2 (Cy). **Anal.** Calcd for $C_{17}H_{24}N_2O_2$ (288.39 gmol^{-1}): C, 70.80; H, 8.39; N, 9.71. Found: C, 69.98; H, 8.40; N, 9.57.

[Rh(IBiox6)$_3$][BAr$^F_4$] (Rh3-Cy)

To a mixture of $[Rh(COE)_2Cl]_2$ (0.036 g, 0.05 mmol), IBiox6 (0.094 g, 0.325 mmol) and Na[$BArF_4$] (0.093 g, 0.105 mmol) was added 1,2-$C_6H_4F_2$ (3.0 mL). The resulting suspension was stirred for 1 hour at room temperature, diluted with heptane (1.0 mL) and filtered. Layering the filtrate with heptane gave the crude product upon diffusion. Recrystallisation from 1,2-$C_6H_4F_2$ – heptane afforded the analytically pure product. Yield = 0.126 g (69%, purple crystals).

Solution stability was tested using a solution of **Rh3-Cy** (0.018 g, 0.01 mmol) in CD_2Cl_2 and 1,2-$C_6H_4F_2$ (0.5 mL) in a J Young's valve NMR tube. In both cases no significant change was observed after 48 hours by ^{1}H NMR spectroscopy.

^{1}H NMR (1,2-$C_6H_4F_2$/C_6D_6, 400 MHz): δ 8.11 – 8.16 (m, 8H, Ar^F), 7.49 (br, 4H, Ar^F), 4.42 (d, $^2J_{HH}$ = 8.8, 6H, OCH_2), 4.38 (d, $^2J_{HH}$ = 8.8, 6H, OCH_2), 3.55 (td, $^3J_{HH}$ = 13.7, 4.0, 6H, Cy), 2.08 (d, $^2J_{HH}$ = 12.9, 6H, Cy), 1.84 (d, $^2J_{HH}$ = 14.2, 6H, Cy), 1.53 (d, $^2J_{HH}$ = 9.6, 6H, Cy), 1.46 (d, $^2J_{HH}$ = 11.2, 12H, Cy), 1.21 (app q, J = 14, 6H, Cy), 1.06

(app q, *J* = 11, 12H, Cy), 0.88 (app t, *J* = 11, 6H, Cy). **^{1}H NMR** (CD_2Cl_2, 500 MHz): δ 7.70 – 7.74 (m, 8H, Ar^F), 7.57 (br, 4H, Ar^F), 4.60 (d, $^2J_{HH}$ = 8.6, 6H, OCH_2), 4.53 (d, $^2J_{HH}$ = 8.6, 6H, OCH_2), 3.56 (td, $^3J_{HH}$ = 13.6, 4.4, 6H, Cy), 2.18 (app d, *J* = 12, 6H, Cy), 1.95 (app d, *J* = 14, 6H, Cy), 1.71 (app d, *J* = 14, 6H, Cy), 1.64 (app d, *J* = 11, 12H, Cy), 1.36 (qt, $^3J_{HH}$ = 14.1, 3.8, 6H, Cy), 1.24 (qt, $^3J_{HH}$ = 13.4, 3.4, 6H, Cy), 1.09 (qt, $^3J_{HH}$ = 13.3, 3.7, 6H, Cy), 0.91 (td, $^3J_{HH}$ = 12.6, 4.3, 6H, Cy). **^{13}C{^{1}H} NMR** (CD_2Cl_2, 126 MHz): δ 162.3 (q, $^1J_{BC}$ = 50, Ar^F), 154.9 (d, $^1J_{IrC}$ = 66, NCN), 135.4 (s, Ar^F), 129.4 (qq, $^2J_{FC}$ = 32, $^3J_{BC}$ = 3, Ar^F), 127.0 (s, $\underline{C}OCH_2$), 125.2 (q, $^1J_{FC}$ = 272, Ar^F), 118.0 (sept, $^3J_{FC}$ = 4, Ar^F), 83.4 (s, OCH_2), 66.9 (s, $COCH_2\underline{C}$)), 35.2 (s, Cy), 34.7 (s, Cy), 24.5 (s, Cy), 24.1 (s, Cy), 24.1 (s, Cy). **Anal.** Calcd for $C_{83}H_{84}BF_{24}N_6O_6Rh$ (1831.30 $gmol^{-1}$): C, 54.44; H, 4.62; N, 4.59. Found: C, 54.49; H, 4.70; N, 4.61.

Computational details

Geometry optimizations without symmetry constraints were carried out using the Gaussian09[26] optimizer (standard convergence criteria) combined with Turbomole (version 6.4)[27] energies and gradients (SCF convergence criterion 10^{-8} a.u., grid m4). Density functional theory was used with the GGA functional BP86[28], the def2-TZVPP[29] basis set and considering dispersion corrections with the DFT-D3 scheme.[30]

Starting from these structures, subsequent optimization for the bonding analysis part was carried out with the same functional and the TZ2P basis set as implemented in the ADF 2013 package.[31] Characterization of stationary points as minima on the potential energy surface was verified by computation of the Hessian matrix. Complex **Rh3-Cy'** was investigated on the more efficient BP86-D3/def2-TZVPP level of approximation only.

To shed light on the bonding situation in the complexes, the *energy decomposition analysis* (EDA)[32] was carried out with the same approach (BP86/TZ2P plus DFT-D3). The EDA investigates the bonding energy for the interaction of two fragments A and B forming an entity AB by separating the bond formation process into several sub-steps. The bond energy ΔE_{bond} is given by a sum of promotion and interaction energy:

$$\Delta E_{bond} = \Delta E_{prep} + \Delta E_{int} \qquad (1)$$

Necessary geometric distortion and electronic excitation of the fragments to form the bond lead to ΔE_{prep}. The intrinsic interaction energy ΔE_{int} can than further be divided in three parts, which are derived successively:

$$\Delta E_{int} = \Delta E_{elstat} + \Delta E_{Pauli} + \Delta E_{orb} \qquad (2)$$

The first term (ΔE_{elstat}) represents the quasiclassical electrostatic interaction energy between the two charge distributions and results in a product wave function $\{\Psi_A\Psi_B\}$. The second term (ΔE_{Pauli}) is a consequence of the antisymmetrization and normalization required after the first step leading to the intermediate wave function Ψ_0 and is associated with steric repulsion. In the final step, Ψ_0 is fully relaxed to the optimal wavefunction Ψ_{AB} for the molecule. This results in an orbital interaction term ΔE_{orb}. This last term is associated with the deformation density $\Delta\rho$ from Ψ_0 to Ψ_{AB} can further be represented in Natural

Orbitals for Chemical Valence (NOCV).[33] This leads to pairs of complementary orbitals (ψ_{-k}, ψ_k) with eigenvalues $\pm v_k$ which have the same value but opposite sign. From these NOCV orbitals N/2 (N = number of electrons) deformation densities $\Delta\rho_k$ can be derived to build up the full deformation density $\Delta\rho$.

$$\Delta\rho = \sum_{k=1}^{N/2} v_k[-\psi_{-k}^2 + \psi_k^2] = \sum_{k=1}^{N/2} \Delta\rho_k \qquad (3)$$

The eigenvalues $\pm v_k$ represent the amount of charge transferred between the fragments in the deformation density and the deformation densities $\Delta\rho_k$ allow a characterization of the interaction. Furthermore, it is possible to assign an energy value to each $\Delta\rho_k$, which sums up to ΔE_{orb}.

$$\Delta E_{orb} = \sum_{k=1}^{N/2} \Delta E_k^{orb} \qquad (4)$$

More details regarding the EDA and EDA-NOCV can be found in the literature.[34]

Supporting information

Structure and EDA of an alternative conformer of **Rh3-H2'** (Figure S1 and Table S1), selected NMR spectra, Cartesian coordinates and SCF energies for all optimised structures. This material is available free of charge via the Internet at http://pubs.acs.org. Full crystallographic details including solution, refinement and disorder modelling procedures are document in CIF format and have been deposited with the Cambridge Crystallographic Data Centre under CCDC 1408318 (**Ir2**), 1408319 (**Ir5**) and 1408320 (**Rh3-Cy**)

Acknowledgements

The authors thank the Swiss National Science Foundation (S.A.H.) and the Royal Society (A.B.C.) for financial support. R.T. thanks the University of Warwick for an IAS Residential Fellowship and the HRZ Marburg for access to computational resources. Crystallographic data was collected using a diffractometer purchased through support from Advantage West Midlands and the European Regional Development Fund.

Notes

The authors declare no competing financial interest.

References

[1] (a) Díez-González, S.; Marion, N.; Nolan, S. P. *Chem. Rev.* **2009**, *109*, 3612–3676; (b) Samojłowicz, C.; M.; Grela, K. *Chem. Rev.* **2009**, *109*, 3708–3742; (c) Hahn, F. E.; Jahnke, M. C. *Angew. Chem. Int. Ed.* **2008** *47*, 3122–3172; (d) Hopkinson, M. N.; Richter, C.; Schedler, M.; Glorius, F. *Nature* **2014**, *510*, 485–496.

[2] Jacobsen, H.; Correa, A.; Poater, A.; Costabile, C.; Cavallo, L. *Coord. Chem. Rev.* **2009**, *253*, 687-703.

[3] Early discussions emphasising the importance of aromaticity and the neglect of π-bonding contributions are nowadays settled: (a) Jacobsen, H., *J. Chem. Soc., Dalton Trans.* **2006**, 2214-2224; (b) Sanderson, M. D.; Kamplain, J. W.; Bielawski, C. W., *J. Am. Chem. Soc.* **2006,** *128*, 16514-16515; (c) Boehme, C.; Frenking, G., *J. Am. Chem. Soc.* **1996,** *118*, 2039-2046; (d) Heinemann, C.; Müller, T.; Apeloig, Y.; Schwarz, H., *J. Am. Chem. Soc.* **1996,** *118*, 2023-2038.

[4] (a) Dröge, T.; Glorius, F. *Angew. Chem. Int. Ed.* **2010**, *49*, 6940–6952; (b) Herrmann, W. A.; Schütz, J.; Frey, G. D.; Herdtweck, E., *Organometallics* **2006,** *25*, 2437-2448.

[5] Frenking, G.; Fröhlich, N. *Chem. Rev.* **2000**, *100*, 717-774.

[6] (a) Gusev, D. G. *Organometallics* **2009**, *28*, 6458-6461; (b) Tonner, R.; Frenking, G. *Organometallics* **2009**, *28*, 3901-3905; (c) Kelly, R. A., III; Clavier, H.; Giudice, S.; Scott, N. M.; Stevens, E. D.; Bordner, J.; Samardjiev, I.; Hoff, C. D.; Cavallo, L.; Nolan, S. P. *Organometallics* **2008**, *27*, 202–210; (d) Chianese, A. R.; Li, X.; Janzen, M. C.; Faller, J. W.; Crabtree, R. H. *Organometallics* **2003**, *22*, 1663–1667.

[7] (a) Tonner, R.; Frenking, G. *Chem.-Eur. J.* **2008**, *14*, 3273-3289; (b) Tonner, R.; Heydenrych, G.; Frenking, G. *Chem.-Asian J.* **2007**, *2*, 1555-1567.

[8] Benhamou, L.; Bastin, S.; Lugan, N.; Lavigne, G.; César, V. *Dalton Trans.* **2014**, *43*, 4474–4482.

[9] (a) Higelin, A.; Keller, S.; Göhringer, C.; Jones, C.; Krossing, I. *Angew. Chem. Int. Ed.* **2013**, *52*, 4941–4944; (b) Schumann, H.; Gottfriedsen, J.; Glanz, M.; Dechert, S.; Demtschuk, J. *J. Organomet. Chem.* **2001**, *617-618*, 588–600.

[10] Dastgir, S.; Coleman, K. S.; Cowley, A. R.; Green, M. L. H. *Dalton Trans.* **2009**, 7203–7214.

[11] For interesting distorted NHC geometries resulting from additional π-coordination of the *N*-aryl substituents to the metal centre see: Kolychev, E. L.; Kronig, S.; Brandhorst, K.; Freytag, M.; Jones, P. G.; Tamm, M. *J. Am. Chem. Soc.* **2013**, *135*, 12448–12459.

[12] (a) Glorius, F.; Altenhoff, G.; Goddard, R.; Lehmann, C. *Chem. Commun.* **2002**, 2704–2705; (b) Altenhoff, G.; Goddard, R.; Lehmann, C. W.; Glorius, F. *Angew. Chem. Int. Ed.* **2003**, *42*, 3690–3693; (c) Altenhoff, G.; Goddard, R.; Lehmann, C. W.; Glorius, F. *J. Am. Chem. Soc.* **2004**, *126*, 15195–15201; (d) G. Altenhoff, S. Würtz, F. Glorius, *Tetrahedron Lett.* **2006**, *47*, 2925-2928; (e) Würtz, S.; Lohre, C.; Fröhlich, R.; Bergander, K.; Glorius, F. *J. Am. Chem. Soc.* **2009**, *131*, 8344–8345; (f) C. Lohre, C. Nimphius, M. Steinmetz, S. Würtz, R. Fröhlich, C. G. Daniliuc, S. Grimme, F. Glorius, *Tetrahedron* **2012**, *68*, 7636-7644.

[13] Crudden, C. M.; Allen, D. P. *Coord. Chem. Rev.* **2004**, *248*, 2247–2273. For other representative examples

see: (a) Jazzar, R. F. R.; Macgregor, S. A.; Mahon, M. F.; Richards, S. P.; Whittlesey, M. K. *J. Am. Chem. Soc.* **2002**, *124*, 4944–4945; (b) Ohki, Y.; Hatanaka, T.; Tatsumi, K. *J. Am. Chem. Soc.* **2008**, *130*, 17174–17186; (c) Navarro, J.; Torres, O.; Martín, M.; Sola, E. *J. Am. Chem. Soc.* **2011**, *133*, 9738–9740; (d) Phillips, N.; Rowles, J.; Kelly, M. J.; Riddlestone, I.; Rees, N. H.; Dervisi, A.; Fallis, I. A.; Aldridge, S. *Organometallics* **2012**, *31*, 8075–8078; (e) Wheatley, J. E.; Ohlin, C. A.; Chaplin, A. B. *Chem. Commun.* **2014**, *50*, 685–687.

[14] (a) Caddick, S.; Cloke, F. G. N.; Hitchcock, P. B.; de K. Lewis, A. K. *Angew. Chem. Int. Ed.* **2004**, *43*, 5824–5827; (b) Bramananthan, N.; Mas-Marzá, E.; Fernández, F. E.; Ellul, C. E.; Mahon, M. F.; Whittlesey, M. K. *Eur. J. Inorg. Chem.* **2012**, 2213–2219; (c) Dorta, R.; Stevens, E. D.; Nolan, S. P. *J. Am. Chem. Soc.* **2004**, *126*, 5054–5055; (d) Scott, N. M.; Pons, V.; Stevens, E. D.; Heinekey, D. M.; Nolan, S. P. *Angew. Chem. Int. Ed.* **2005**, *44*, 2512–2515; (e) Scott, N. M.; Dorta, R.; Stevens, E. D.; Correa, A.; Cavallo, L.; Nolan, S. P. *J. Am. Chem. Soc.* **2005**, *127*, 3516–3526; (f) Zenkina, O. V.; Keske, E. C.; Wang, R.; Crudden, C. M. *Organometallics* **2011**, *30*, 6423–6432; (g) Rivada-Wheelaghan, O.; Donnadieu, B.; Maya, C.; Conejero, S. *Chem. Eur. J.* **2010**, *16*, 10323–10326.

[15] (a) Chaplin, A. B. *Organometallics* **2014**, *33*, 624–626; (b) Chaplin, A. B. *Organometallics* **2014**, *33*, 3069–3077.

[16] Hauser, S. A.; Prokes, I.; Chaplin, A. B. *Chem. Commun.* **2015**, *51*, 4425 - 4428.

[17] Based on the small electronic and structural differences between the conformations detailed in the preceding section, no significant differences could be expected in these mono-ligated systems containing only co-ligands with small steric profiles.

[18] The computed values for pitching and yawing movements were fitted with 2^{nd} and 4^{th} order polynomials, respectively. Pitching: $y = a_0+a_1x+a_2x^2$; Rh: $a_0 = 0.50035$, $a_1 = 0.03844$, $a_2 = 0.03745$, $R^2 = 0.9977$; Ir: $a_0 = 0.40783$, $a_1 = 0.02069$, $a_2 = 0.03884$, $R^2 = 0.9992$. Yawing: $y = a_0+a_1x+a_2x^2+a_3x^3+a_4x^4$; Rh: $a_0 = 0.87467$, $a_1 = 0.00047$, $a_2 = 0.09631$, $a_3 = 0$, $a_4 = 0.00014$, $R^2 = 0.9999$; Ir: $a_0 = 0.84552$, $a_1 = 0.00010$, $a_2 = 0.11462$, $a_3 = 0$, $a_4 = 0.00016$, $R^2 = 0.9999$.

[19] Nelson, D. J.; Truscott, B. J.; Slawin, A. M. Z.; Nolan, S. P. *Inorg. Chem.* **2013**, *52*, 12674–12681.

[20] See, for example: (a) Tang, C. Y.; Smith, W.; Vidovic, D.; Thompson, A. L.; Chaplin, A. B.; Aldridge, S. *Organometallics* **2009**, *28*, 3059–3066; (b) Collman, J. P.; Hegedus, L. S.; Norton, J. R.; Finke, R. G. *Principles and Applications of Organotransition Metal Chemistry*; University Science Books: Sausalito, CA, 1987; (c) Albright, T. A.; Burdett, J. K.; Whangbo, M.-H. *Orbital Interactions in Chemistry*; Wiley-Interscience: Chichester, 1985.

[21] As a consequence of the relative twisting of the NHC ligands about the $M–C_{NCN}$ vector, these tris-NHC complexes are chiral.

[22] Brookhart, M.; Green, M. L. H.; Parkin, G. *PNAS* **2007**, *104*, 6908–6914.

[23] Tapu, D.; Dixon, D. A.; Roe, C. *Chem. Rev.* **2009**, *109*, 3385–3407.

[24] van der Ent, A.; Onderdelinden, A. L.; Schunn, R. A. *Inorg. Synth.* **1990**, *28*, 90–92.

[25] Buschmann, W. E.; Miller, J. S.; Bowman-James, K.; Miller, C. N. *Inorg. Synth.* **2002**, *33*, 83–91.

[26] Frisch, M. J.; Trucks, G. W.; Schlegel, H. B.; Scuseria, G. E.; Robb, M. A.; Cheeseman, J. R.; Scalmani, G.; Barone, V.; Mennucci, B.; Petersson, G. A.; Nakatsuji, H.; Caricato, M.; Li, X.; Hratchian, H. P.; Izmaylov, A. F.; Bloino, J.; Zheng, G.; Sonnenberg, J. L.; Hada, M.; Ehara, M.; Toyota, K.; Fukuda, R.; Hasegawa, J.; Ishida, M.; Nakajima, T.; Honda, Y.; Kitao, O.; Nakai, H.; Vreven, T.; Montgomery Jr., J. A.; Peralta, J. E.; Ogliaro, F.; Bearpark, M. J.; Heyd, J.; Brothers, E. N.; Kudin, K. N.; Staroverov, V. N.; Kobayashi, R.; Normand, J.; Raghavachari, K.; Rendell, A. P.; Burant, J. C.; Iyengar, S. S.; Tomasi, J.; Cossi, M.; Rega, N.; Millam, N. J.; Klene, M.; Knox, J. E.; Cross, J. B.; Bakken, V.; Adamo, C.; Jaramillo, J.; Gomperts, R.; Stratmann, R. E.; Yazyev, O.; Austin, A. J.; Cammi, R.; Pomelli, C.; Ochterski, J. W.; Martin, R. L.; Morokuma, K.; Zakrzewski, V. G.; Voth, G. A.; Salvador, P.; Dannenberg, J. J.; Dapprich, S.; Daniels, A. D.; Farkas, Ö.; Foresman, J. B.; Ortiz, J. V.; Cioslowski, J.; Fox, D. J. Gaussian 09, Revision C.01, Gaussian, Inc.: Wallingford, CT, USA, 2009.

[27] (a) Ahlrichs, R.; Bär, M.; Häser, M.; Horn, H.; Kölmel, C., *Chem. Phys. Lett.* **1989,** *162*, 165-9; (b) Turbomole, 6.4, 2014, a development of University of Karlsruhe and Forschungszentrum Karlsruhe GmbH, 1989-2007, Turbomole GmbH, since 2007; available from http://www.turbomole.com (last accessed 27.07.2015).

[28] (a) Perdew, J., *Phys. Rev. B* **1986**, 8822-8824; (b) Becke, A., *Phys. Rev. A* **1988,** *38*, 3098-3100.

[29] Weigend, F.; Ahlrichs, R., *Phys. Chem. Chem. Phys.* **2005,** *7*, 3297-3305.

[30] (a) Grimme, S.; Antony, J.; Ehrlich, S.; Krieg, H., *J. Chem. Phys.* **2010,** *132*, 154104; (b) Grimme, S.; Ehrlich, S.; Goerigk, L., *J. Comput. Chem.* **2011,** *32*, 1456-1465.

[31] (a) Te Velde, G.; Bickelhaupt, F. M.; Baerends, E. J.; Fonseca Guerra, C.; Van Gisbergen, S. J. A.; Snijders, J. G.; Ziegler, T., *J. Comp. Chem.* **2001,** *22*, 931-967; (b) Fonseca Guerra, C.; Snijders, J. G.; Te Velde, G.; Baerends, E. J., *Theor. Chem. Acc.* **1998,** *99*, 391-403; (c) ADF2013, SCM, Theoretical Chemistry, Vrije Universiteit, Amsterdam, The Netherlands, http://www.scm.com (last accessed 27.07.2015).

[32] (a) Kitaura, K.; Morokuma, K., *Int. J. Quantum Chem.* **1976,** *X*, 325-340; (b) Ziegler, T.; Rauk, A., *Theor. Chim. Acta* **1977,** *46*, 1-10.

[33] (a) Mitoraj, M.; Michalak, A., *J. Mol. Model.* **2007,** *13*, 347-355; (b) Mitoraj, M. P.; Michalak, A.; Ziegler, T., *J. Chem. Theory Comput.* **2009,** *5*, 962-975.

[34] (a) Mitoraj, M. P.; Michalak, A.; Ziegler, T., *Organometallics* **2009,** *28*, 3727-3733; (b) Mitoraj, M. P., *J. Phys. Chem. A* **2011,** *115*, 14708-14716; (c) Ndambuki, S.; Ziegler, T., *Inorg. Chem.* **2012,** *51*, 7794-7800.; (c) Hopffgarten, M. v.; Frenking, G., *WIREs Comput. Mol. Sci.* **2012,** *2*, 43-62; (d) Frenking, G.; Krapp, A., *J. Comput. Chem.* **2007,** *28*, 15-24; (e) Krapp, A.; Bickelhaupt, F. M.; Frenking, G., *Chem.--Eur. J.* **2006,** *12*, 9196-9216; (f) Raupach, M.; Dehnen, S.; Tonner, R., *J. Comput. Chem.* **2014,** *35*, 1045-1057; (h) Raupach, M.; Tonner, R., *J. Chem. Phys.* **2015,** *142*, 194105.